UNCLASSIFIED

RANRL T/N (EXT) No 1/83

AR Number: 002-707

DEPARTMENT OF DEFENCE

DEFENCE SCIENCE AND TECHNOLOGY ORGANISATION

R.A.N. RESEARCH LABORATORY

EDGECLIFF, N.S.W.

RANRL TECHNICAL NOTE

(EXTERNAL) No 1/83

A COMPUTER PROGRAM FOR THE PREDICTION OF SEARCH RADAR PERFORMANCE

M.R.BATTAGLIA

APPROVED FOR PUBLIC RELEASE

COPY No. 23

March 1983

UNCLASSIFIED

83 08 03 012

UNCLASSIFIED

DEPARTMENT OF DEFENCE

R.A.N. RESEARCH LABORATORY

RANRL TECHNICAL NOTE (EXTERNAL) No 1/83

A COMPUTER PROGRAM FOR THE PREDICTION OF SEARCH RADAR PERFORMANCE

M.R.BATTAGLIA

ABSTRACT

A computer program is described which calculates signal and clutter return and probability of detection for scanning search radars. Sample outputs are plotted showing the effects of humidity, sea state and target scintillation.

POSTAL ADDRESS: The Director, RAN Research Laboratory
P.O. Box 706 Darlinghurst, N.S.W. 2010

CONTENTS

1. INTRODUCTION	1
2. GENERAL BACKGROUND	1
2.1 The Radar Equation	1
2.2 System Noise Power	2
2.3 Atmospheric Losses	4
2.4 Miscellaneous Losses	7
3. PATTERN PROPAGATION FACTOR	9
3.1 General Procedure	9
3.2 Reflectivity	10
4. NON-STANDARD ATMOSPHERIC CONDITIONS	16
4.1 Humidity	16
4.2 Sea State	16
5. PROBABILITY OF DETECTION	19
ACKNOWLEDGEMENTS	25
REFERENCES	31

LIST OF ANNEXES

I Antenna Pattern Functions	32
II Probability of Detection Subroutines	37
III Solutions to Multipath Geometry	38
DISTRIBUTION	39
DOCUMENT CONTROL DATA SHEET	40

1. INTRODUCTION

The performance of naval radars is routinely checked by measurement of vertical coverage diagrams. This may be accomplished by measuring the signal returned from a target of known radar cross-section flying a constant aspect profile, or from a sphere dropped from a known height and range. Measurements carried under 'standard' conditions can be compared with nominal performance figures as a test of system degradation.

It is not unusual, however, for radar returns several decibels above or below the expected levels (or longer/shorter detection ranges) to be measured without anomalous propagation or system degradation. Much of the discrepancy may be explained in terms of variations in humidity, sea state and the use of different target RCS fluctuation models.

The following sections outline the method and theory behind two computer programs. The first is concerned with the evaluation of signal, clutter and noise levels under specified environmental conditions and target profile. A second program uses these data to calculate probabilities of detection for appropriate scanning parameters, operator/auto-detection and generalized chi-squared target fluctuation models, including Swerling and Weinstock cases. The interactive version of the programs is written in BASIC language and requires 32K bytes of RAM. Execution times are approximately 5 seconds per range point on a Tektronix 4051 Graphics System.

2. GENERAL BACKGROUND

2.1 The Radar Equation

The radar equation relates the returned power at the antenna (P_r) to the transmitted power (P_t) and power gain (G) at wavelength (λ) for a target of cross-section (σ):

$$P_r = \frac{P_t G^2 \sigma \lambda^2 F^4}{(4\pi)^3 R^4 L} \qquad 1.$$

This equation differs from the free space equation by the inclusion of an atmospheric loss factor (L) and the pattern propagation factor (F) which accounts for multipath and diffraction effects. An exponential atmospheric model is assumed, and multipath includes only the direct ray and one indirect ray which is reflected from the sea surface. The geometry is shown in figure 1.

In a dynamic atmosphere F and L are non-uniform in space and time, leading to additional fading effects, however the current model calculates only average values. The only sources of signal fluctuation considered are the radar cross-sections of the target and sea surface.

For a given probability of detection α, usually 50 or 95%, the maximum range R_α for noise-limited detection is

$$R_\alpha = \left[\frac{P_t G^2 \sigma \lambda^2 F^4}{(4\pi)^3 D_o \, L \, P_n} \right]^{0.25} \qquad 2.$$

where P_n is the noise power and D_o is the signal-to-noise ratio required to yield the desired detection and false alarm probabilities. The program assumes Rayleigh amplitude statistics for clutter and receiver noise, so that P_n above can be read as noise-plus-clutter power. Mean clutter power is based on a fit of Nathanson's data (ref 6), and the mean noise level is as described below.

2.2 System Noise Power

Equations 1 and 2 are expressed in terms of powers referred to the antenna, so the noise power P_n is also described by a system temperature T_s referred to the antenna

$$P_n = k \, T_s \, B_n \sim k \, T_s/\tau \qquad 3.$$

where k is Boltzmann's constant, B_n is the noise bandwidth, τ is the effective pulse width, and the system temperature is conveniently expressed in the form used by Blake (Reference 1)

$$T_s = T_a + T_r \, (L_r - 1) + L_r \, T_o \, (NF - 1) \qquad 4.$$

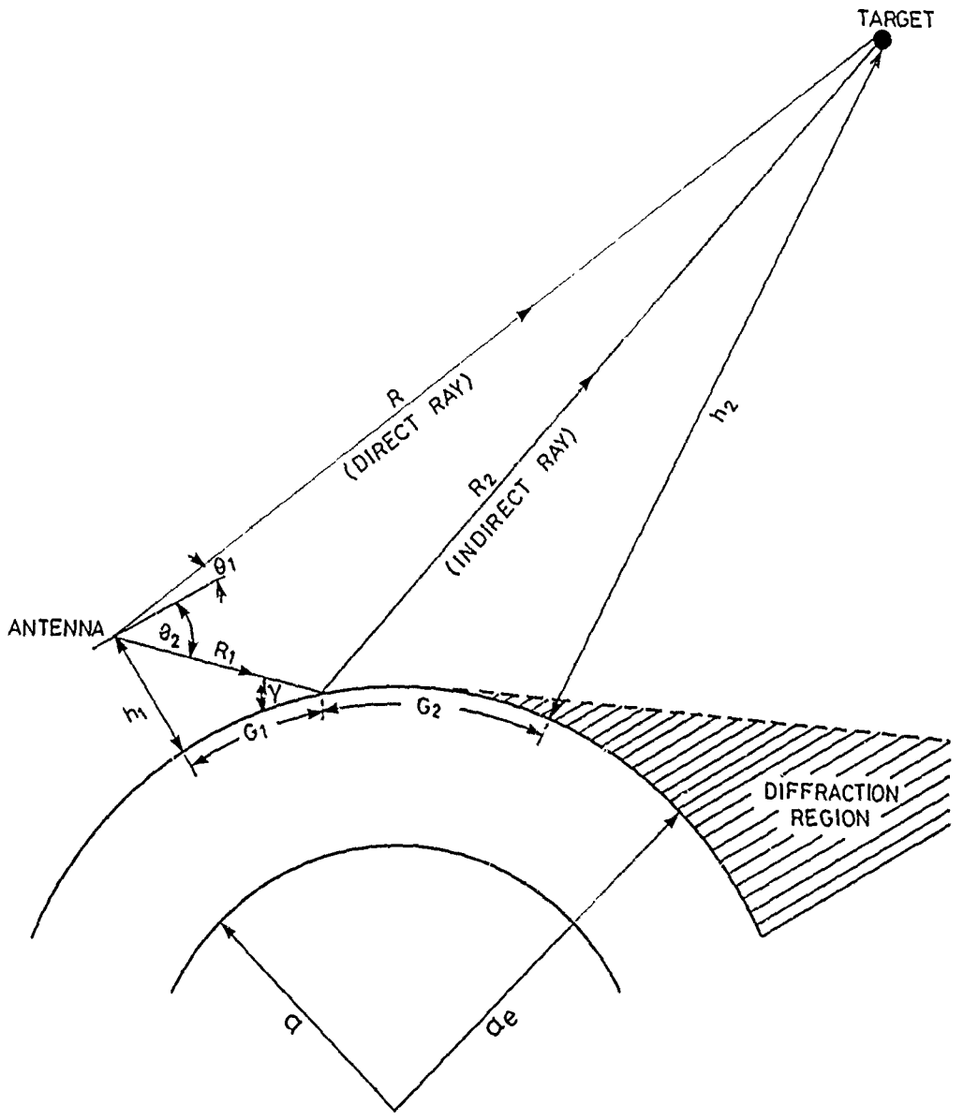

Fig. 1. Illustration of multipath geometry.

in which T_r, L_r, are the receiving line temperature and losses, NF is the receiver noise figure, T_o = 290 and T_a is the antenna temperature. T_a is calculated by an equivalent path (R_{eq}) method

$$T_a = 290 + \{ 10^3/f + 5.8\times10^8/f^{2.5} - 285 \}/(R_{eq}\ \gamma_o) \qquad 5.$$

where f is in MHz, γ_o is the sea-level atmospheric attenuation rate (loss per n.mile) and R_{eq} in n.mile is approximately related to the beam tilt (β)

$$\log_{10}(R_{eq} - 3.5) = 2.03 + 24\log_{10}(1 - 2\beta/\pi) \qquad 6.$$

Antenna temperatures for standard conditions are plotted in figure 2 using equations 5 and 6. These approximations, which are not described elsewhere, agree to within a few degrees with the results of a numerical integration described in reference 2. The atmospheric attenuation is based on the Van Vleck-Weisskopf model for oxygen and water.

2.3 Atmospheric Losses

Atmospheric losses include attenuation by oxygen, water vapour and precipitation. Molecular absorption by water and oxygen is calculated using known intensities and line-widths of the rotational absorption lines. The relative contributions of water and oxygen are shown in figure 3. At UHF frequencies the absorption is dominated by the tail of the 60 GHz absorption band of oxygen, which is calculated using the Van Vleck-Weisskopf model (reference 3) with semi-empirical line-widths (reference 1) to account for band overlap effects.

Many empirical expressions and experimental data exist for rainfall attenuation above 3 GHz (references 1-5), however this is deliberately omitted from the program. At search radar frequencies the attenuation is negligible (10^{-2} - 10^{-3} dB/km) and the incorporation of this loss may introduce errors larger than this figure due to

(i) uncertainty in the cut-off of the cloud base

(ii) inhomogeneity of the rainfall rate over the propagation path and

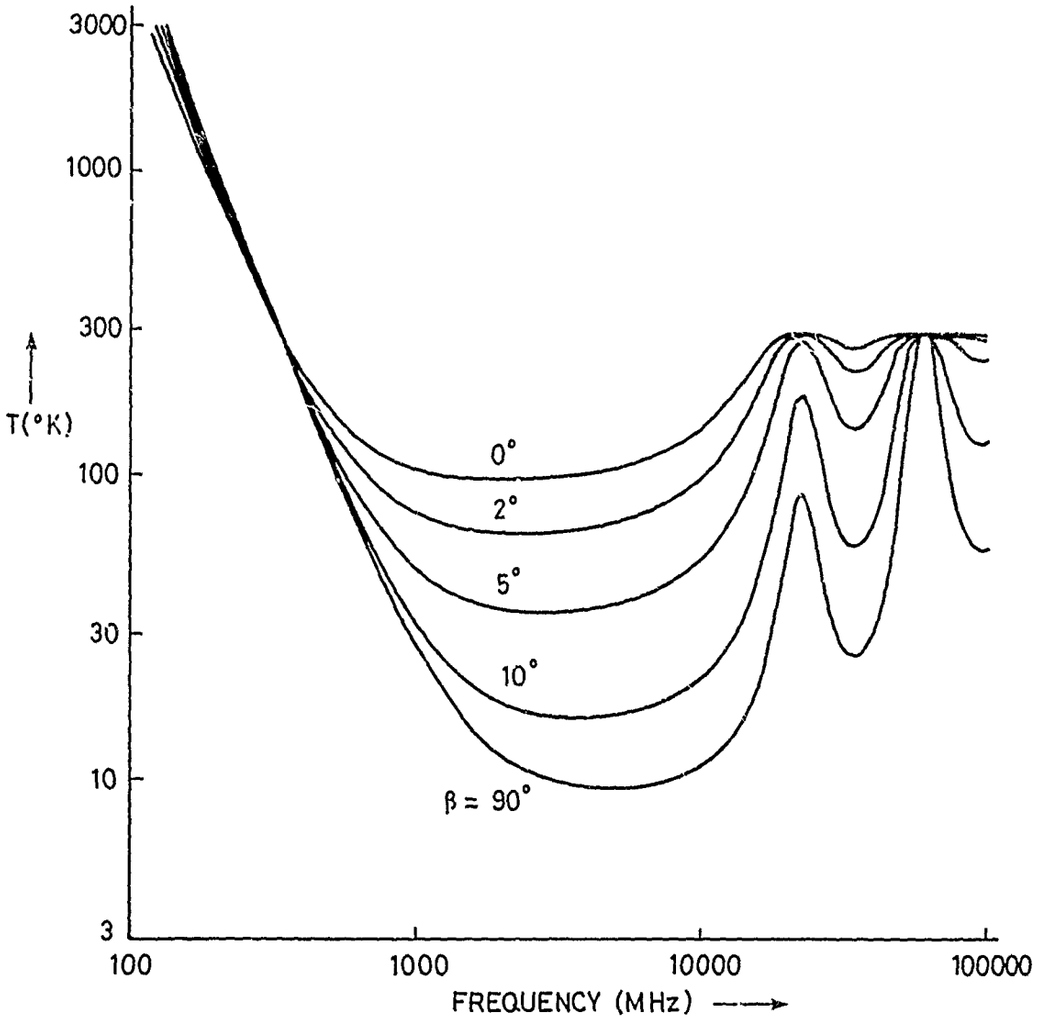

Fig. 2. Temperature (Kelvin) of lossless antenna for elevation angles of 0°, 2°, 5°, 10° and 90°.

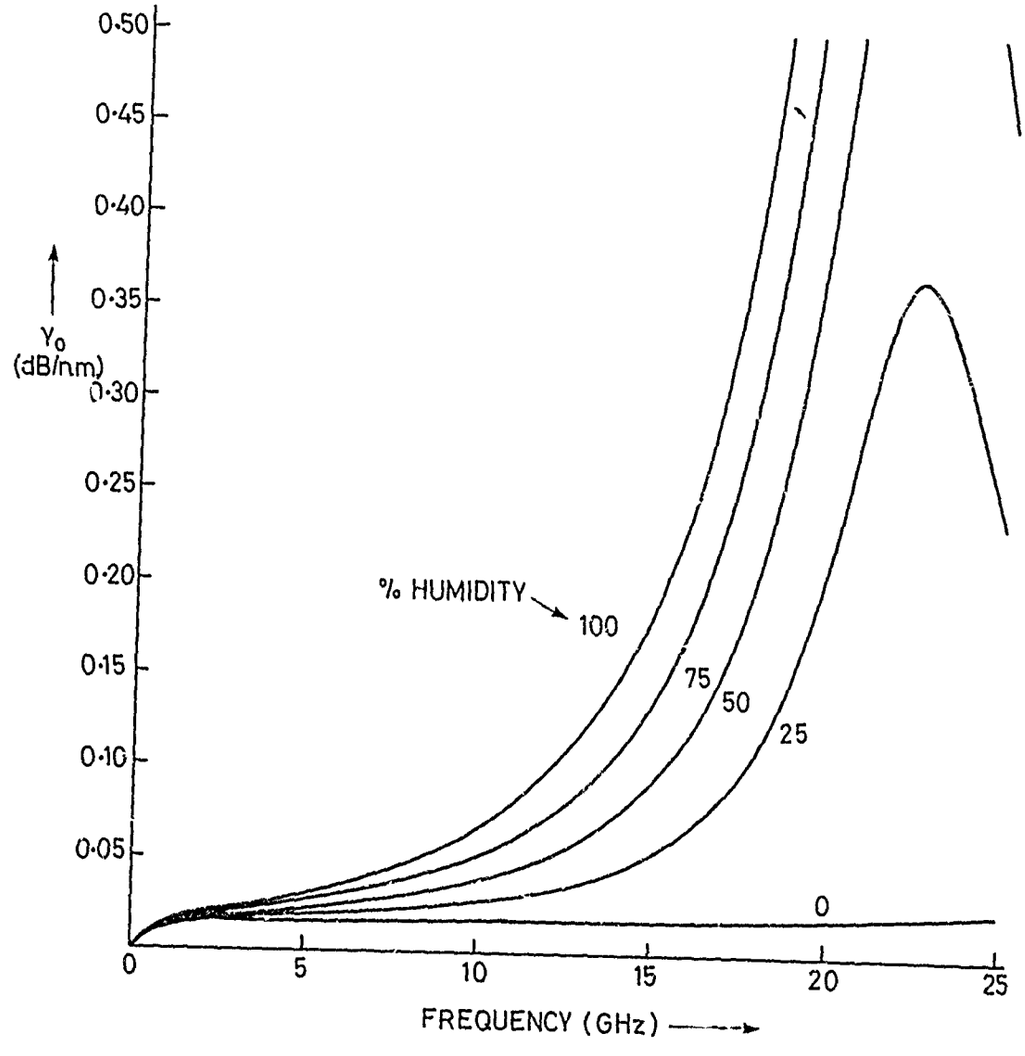

Fig. 3. Atmospheric attenuation (dB/n.mile) at 30° C for 0, 25, 50, 75, and 100% humidity.

(iii) complex frequency-dependence due to

(a) the transition from Mie to Rayleigh turbidity with variable drop-size distribution

(b) rapid dispersion of the dielectric constant of water.

Volume backscatter from rain is more important than attenuation at the frequencies of interest, but this is simply another aspect of the problem described above. Both are treated in the more general radar model of reference 2.

2.4 Miscellaneous Losses

The probability of detection (P_d) can be calculated from the ratio of signal energy to noise power per unit bandwidth. In the program P_d is derived from mean signal-to-noise power ratios, with the assumption of approximately matched pulse spectrum/filter transfer function.

If the mismatch is small it can be included as a loss factor C_b which is calculated from the empirical expression

$$C_b = K \left[\frac{B\tau}{4\alpha}\right] \cdot \left[1 + \frac{\alpha}{B\tau}\right]^2 \qquad 7.$$

where α is the optimum time-bandwidth product ($B\tau$) for the combination of pulse and filter shape, and K is the minimum loss which occurs at $B\tau = \alpha$. Using data from Blake (reference 1) and Barton (reference 4) with equation 7, bandwidth mismatch factors for various pulse/filter combinations have been plotted in figure 4. The default pulse/filter shapes in the program are rectangular/rectangular, and C_b is calculated for either operator- or auto-detection.

A scanning loss factor (1.2 dB) is applied to the signal power, but not the clutter. This is because a beam-shape loss factor has already been included in the calculation of the effective azimuth beamwidth ($\theta_H = 0.75\ \theta_{3dB}$) used to calculate the clutter cell area.

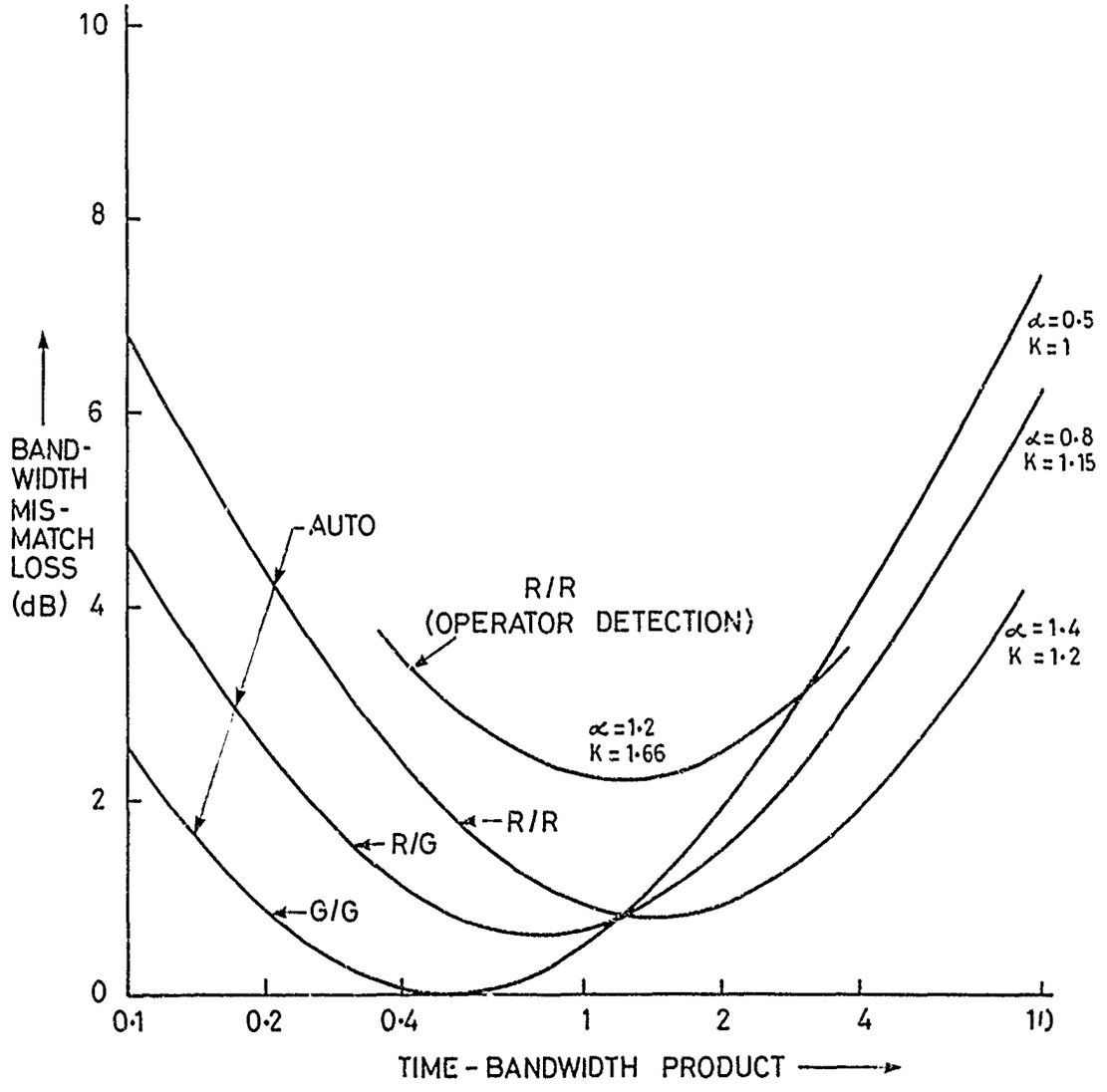

Fig. 4. Bandwidth mismatch loss (dB) for combinations of gaussian (G) and rectangular (R) pulse / filter shapes.

The compressed pulse width of a pulse compession radar can be substituted directly into the radar range equations since the time-bandwidth product equals the pulse compression ratio for a matched filter. A loss must however be included for practical radars where amplitude tapering has been used to reduce the first time/range sidelobe below the 13 dB for a matched filter. The model assumes a 1.5 dB processing loss based on typical weightings (e.g. Hamming or Taylor), time-bandwidth products ($B\tau \sim 50$) and mainlobe pulse broadening (50-60%). This loss is applied to the signal but not the clutter since the target is treated as a point scatterer whereas the clutter 'fills' the resolution cell.

3 PATTERN PROPAGATION FACTOR

3.1 General Procedure

The pattern propagation factor (F) of equation 1 is calculated using (i) ray theory for the interference region, (ii) the single-mode diffraction result well beyond the horizon and (iii) an interpolation procedure near the horizon. A full description of the multipath calculations is given in references 1 and 2 with geometry and symbols as per figure 1. Annex III gives the main geometric approximations used in the BASIC program. The interference lobing structure is given by equation 1 with maxima and minima determined by

$$F = f(\theta_1)(1 \pm x) \qquad 8.$$

where

$$x = \frac{r\ \rho_s\ D\ f(\theta_2)}{f(\theta_1)} \qquad 9.$$

in which $f(\theta_1)$ and $f(\theta_2)$ are the normalized antenna pattern functions for the direct and indirect ray respectively, r is the surface roughness factor, ρ_s is the electromagnetic reflection coefficient and D is the divergence factor.

Beyond the horizon the single-mode diffraction result is used as described in references 1 and 3. At intermediate ranges an exponential

interpolation is used to calculate F. The limits of the intermediate region are:

$$G_{max} = 1.05 \times \text{(radar horizon)}$$

$$G_{min} = \min\left(\pi - 2\gamma_c - \sin^{-1}(a_e \cos\gamma_c/(h_1 + a_e)),\ \sin^{-1}(a_e \cos\gamma_c/(h_2 + a_e))\right) \qquad 10.$$

where

$$\gamma_c = \tan^{-1}(\lambda/2\pi a_e)^{1/3} \qquad 11.$$

Figure 5 is a typical plot of F versus range for a 400 MHz UHF radar showing the interpolation region. The dotted line $F=R/R_\alpha$ is the single-scan detection 'threshold' for a target which is known to have probability α of painting at range R_α in the absence of multipath effects. The single-scan detection range is found at the intersection of this line with the curve for F.

A similar calculation for I-band is shown in figure 6. Here the slight discontinuity in the slope using a simple interpolation (linear in dB versus range) is justified since at higher frequencies clutter-free detection is essentially horizon-limited. Over the UHF/microwave region the interpolation procedure used should introduce negligible additional error in the detection ranges compared with other sources of error.

The clutter return and signal level (1 m^2 target) for the UHF radar and geometry described above is plotted in figure 7 to illustrate the significance of the intermediate region. At the radar horizon the signal-to-noise ratio is -36 dB and increases by only 2 dB/n.mile until unity S/N. In this region the probability of detection is strongly dependent on target RCS fluctuation - the worst case being a steady target.

3.2 Reflectivity

The depth of the nulls and the enhancement due to multipath is determined by the magnitude and phase of the reflected indirect ray. Reflectivity appears in equation 9 as the product of roughness and electromagnetic reflection parameters

$$\Gamma_{\alpha\alpha} = \rho_s \, r \, e^{-j\phi} \qquad 12.$$

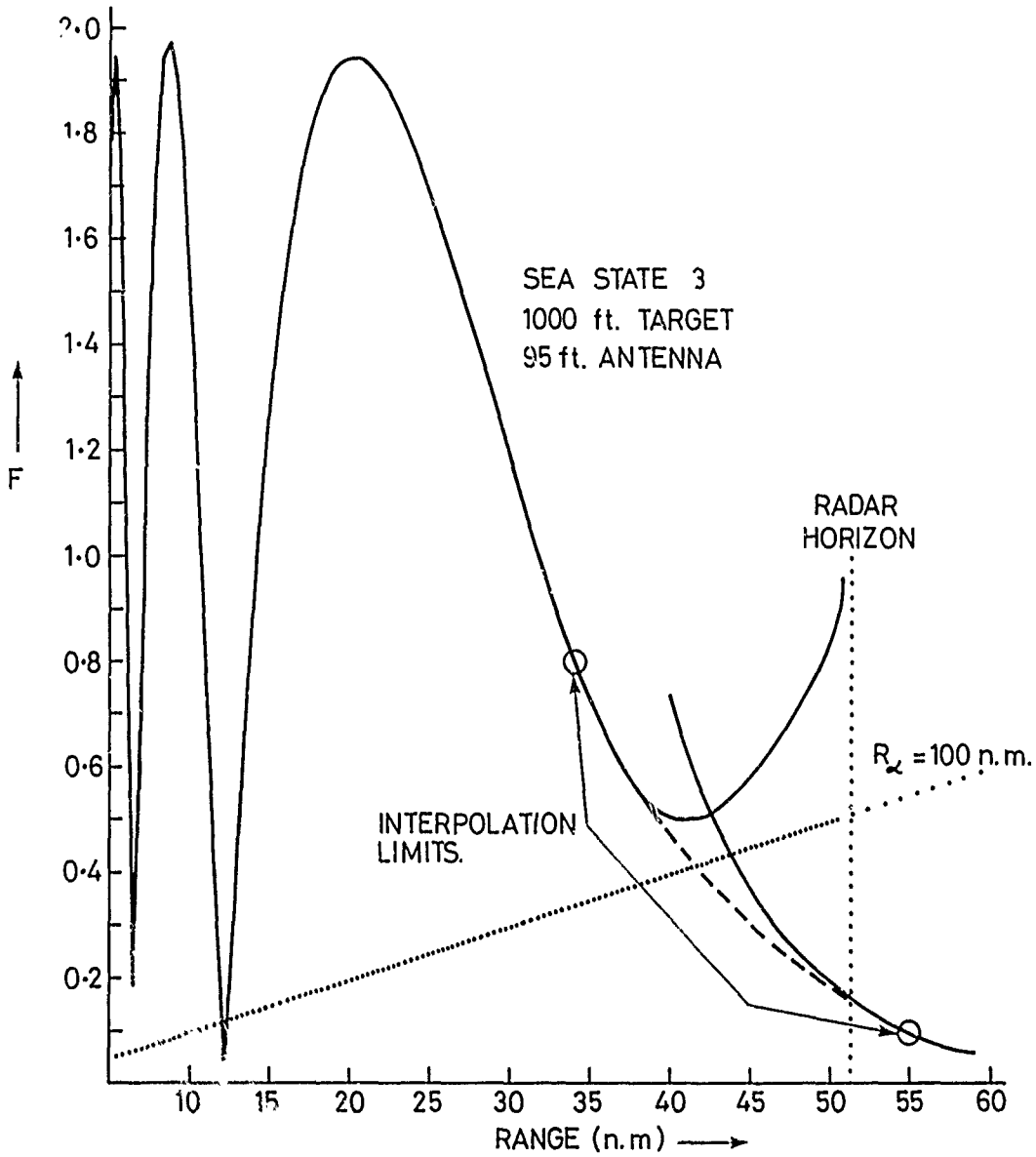

Fig. 5. Pattern propagation factor for shipborne U.H.F. radar.

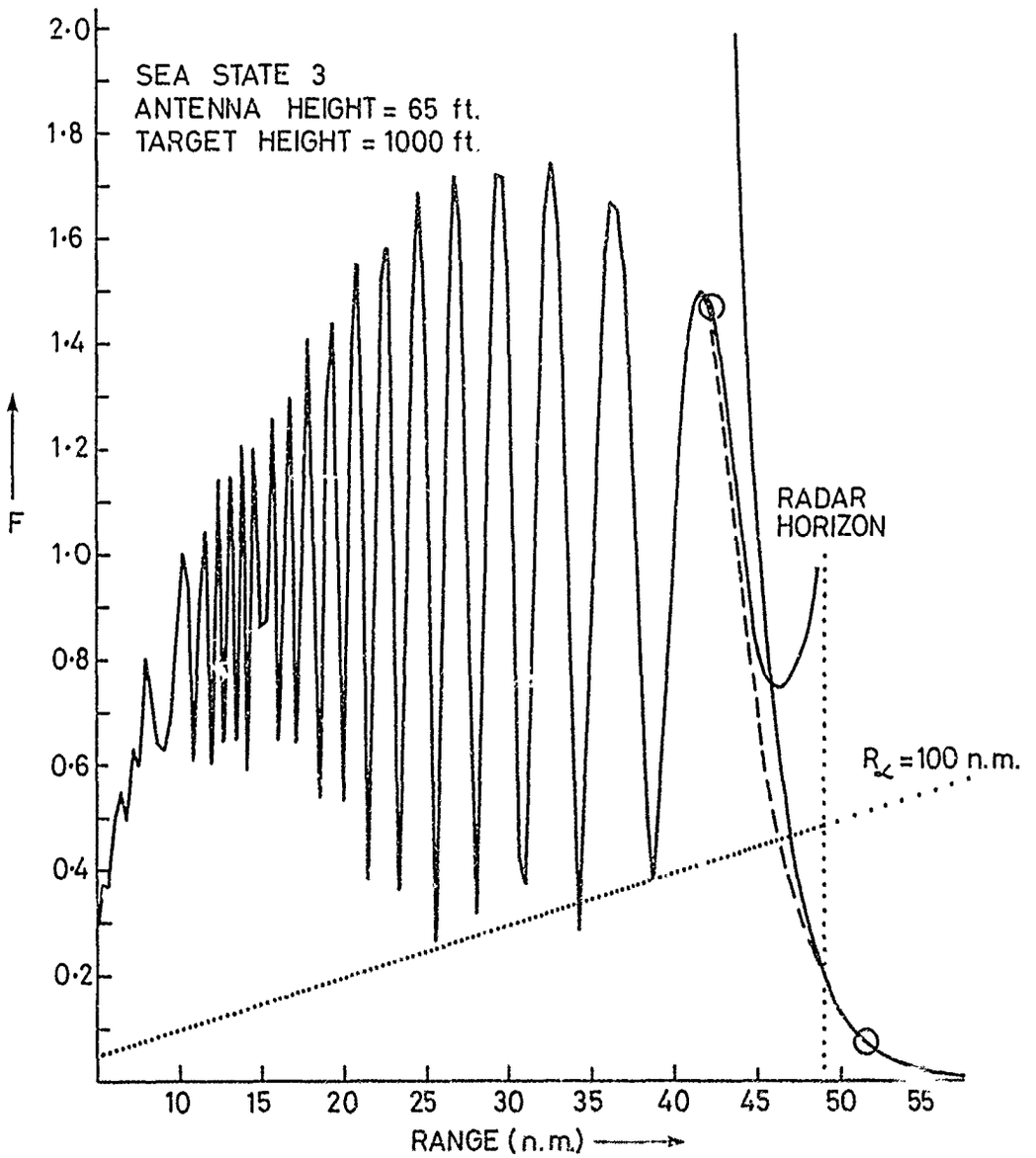

Fig. 6. Pattern propagation factor for shipborne I-band radar.

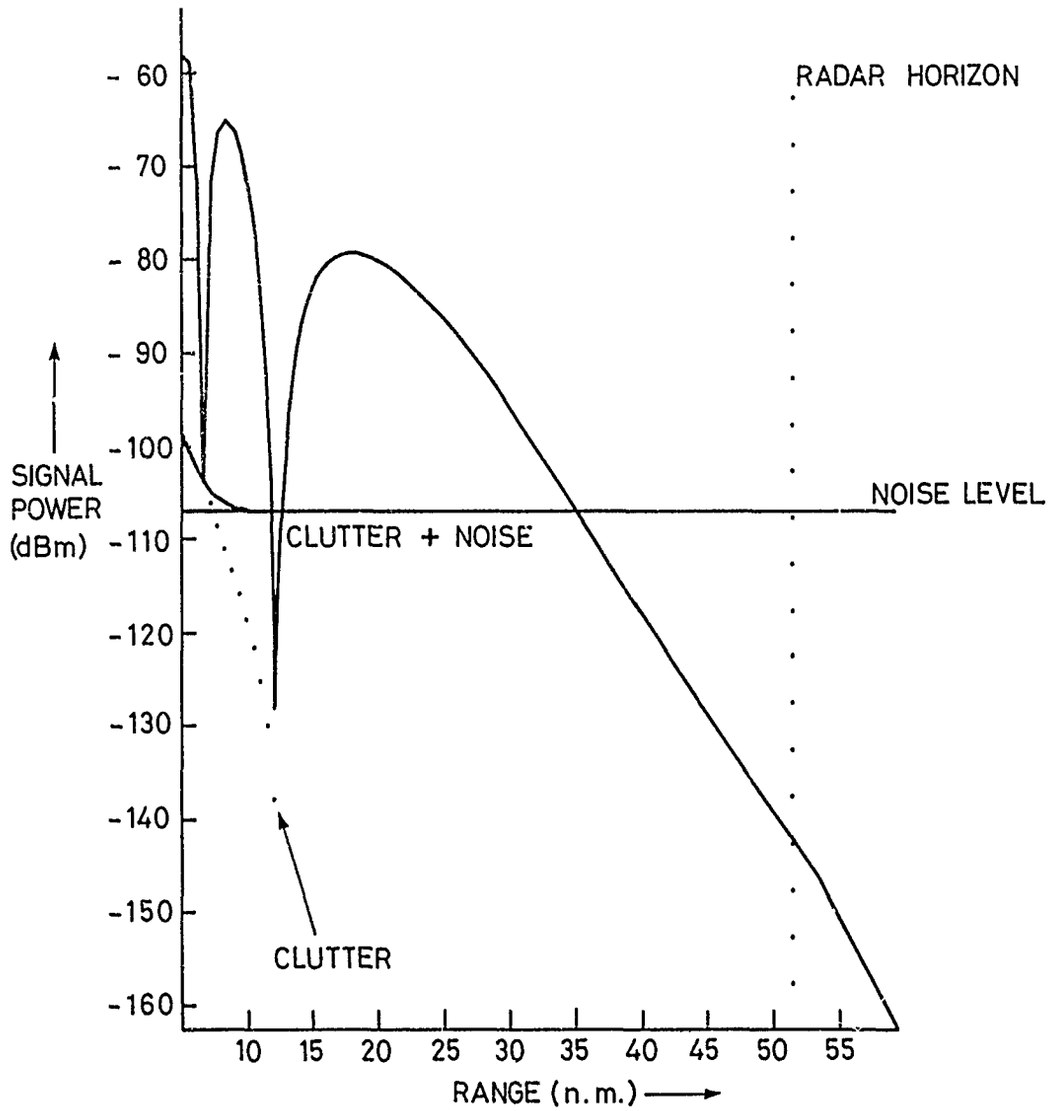

Fig. 7. Signal level (dBm) for radar of fig. 5 standard atmospheric conditions.

where $\alpha\alpha$ = HH or VV represents horizontal or vertical polarization and ϕ is the phase difference on reflection. In the program a semi-empirical expression is used for the roughness factor

$$r = \exp(-2\,s^2) \qquad s<0.6366 \qquad 13a.$$

$$= \exp(-1.2732\,s) \qquad s>0.6366 \qquad 13b.$$

where

$$s = \pi\, H_{1/3}\, \sin\gamma/2\lambda \qquad 14.$$

for significant wave height $H_{1/3}$. Equation 13 is in good agreement with experimental data over the range of grazing angles normally of interest. Figure 8 shows the difference between equations 13a/13b used in the program and the uniform Gaussian shape (equation 13a) used in most radar models. The use of a Gaussian roughness factor leads to an underestimate of multipath lobing at high grazing angles and/or sea states. This difference can be significant even at UHF frequencies.

The electromagnetic part of the reflection coefficient in equation 12 is calculated for each polarization from the expressions

$$(\rho_s e^{-j\phi})_{HH} = \frac{\sin\gamma - (\varepsilon_c - \cos^2\gamma)^{0.5}}{\sin\gamma + (\varepsilon_c - \cos^2\gamma)^{0.5}} \qquad 15a.$$

$$(\rho_s e^{-j\phi})_{VV} = \frac{\varepsilon_c \sin\gamma - (\varepsilon_c - \cos^2\gamma)^{0.5}}{\varepsilon_c \sin\gamma + (\varepsilon_c - \cos^2\gamma)^{0.5}} \qquad 15b.$$

in which ε_c is the complex dielectric constant of sea water at the air-sea interface:

$$\varepsilon_c = \varepsilon_1 - j\varepsilon_2 \qquad 16.$$

with ε_1 and ε_2 being the real and imaginary parts respectively. Default values of interfacial sea water parameters are (i) salinity = 3.4% and (ii) temperature = sea level air temperature. Real and imaginary parts of ε_c are calculated from fits of experimental data from 100 MHz to 100 GHz. Correct allowance for temperature and salinity variations is more important for vertical polarization where the indirect ray grazing angle may be near the quasi-Brewster angle for high-altitude or short-range targets.

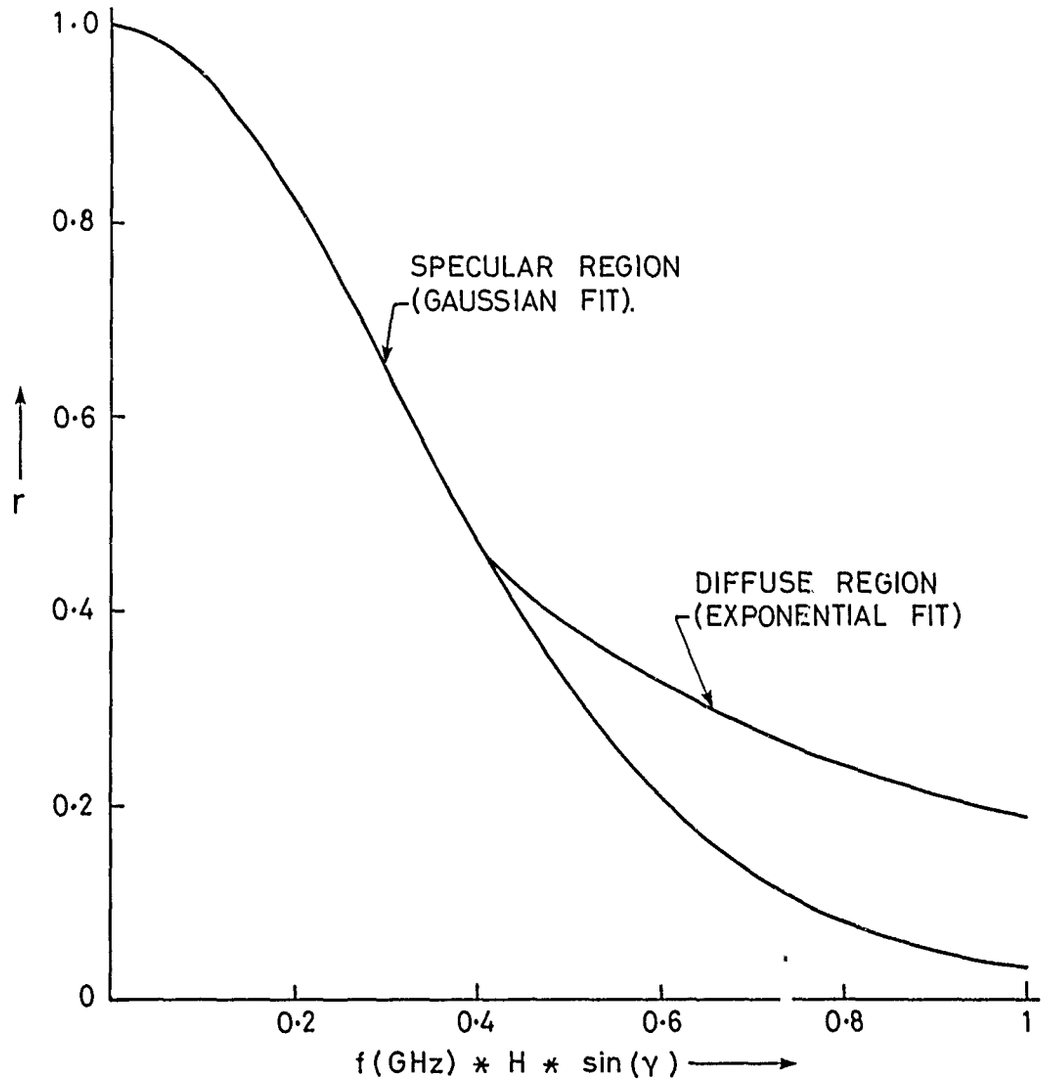

Fig. 8. Surface roughness factor (r) for pure gaussian and gaussian/exponential models.

4 NON-STANDARD ENVIRONMENTAL CONDITIONS

In the absence of ducting or precipitation, the environmental parameters which have the greatest effect on radar performance are humidity and sea state.

4.1 Humidity

Absolute water vapour content is calculated in the program from temperature and relative humidity, using an empirical form of the Clausius-Clapeyron relation (ref 2). A plot of attenuation at various humidities is given in figure 3 for frequencies from 100 MHz to 25 GHz. The effect of humidity is significant only above 1 GHz. At lower frequencies the molecular absorption is dominated by oxygen which has negligible variability at sea level. Absolute humidity and atmospheric pressure are also used, together with molecular polarizations of oxygen, nitrogen and water, to calculate refractivity and hence the effective earth's radius as described in reference 2.

Figures 9 and 10 show the effect of humidity variations on the performance of a hypothetical 5 GHz surface search radar. At high humidity the radar horizon is increased by about 10% as is the peak of the first lobe for a 1000 ft target. The 50% increase in antenna temperature does not show up in the noise level since a high receiver noise figure (10 dB) was used. An additional 1 dB increase in absorption near the horizon is also not apparent due to the simultaneous shift in the lobe structure.

4.2 Sea State

Sea state contributes (i) as a clutter return and (ii) to the multipath lobing through the roughness factor in equation 12. The program assumes a simple relation between significant wave height, in feet, and sea state

$$H_{1/3} = 0.5\ SS^2 \qquad 17.$$

where SS is the Douglas sea state. Figure 20 indicates that this is reasonable for sea states up to 7. The program also accepts non-integer sea states to facilitate the investigation of smaller variations in wave height.

FREQUENCY	=	5000 MHz
PEAK POWER	=	250 kW
RECEIVER NOISE FIGURE	=	10 dB
COMPRESSED PULSE WIDTH	=	1 MICROSEC
RADIATED PULSE WIDTH	=	1 MICROSEC
ANTENNA HEIGHT	=	50 FEET
ANTENNA TILT	=	2 DEGREES
HORIZONTAL BEAM WIDTH	=	1 DEGREE
VERTICAL BEAM WIDTH	=	10 DEGREES
VERTICAL SIDELOBE LEVEL	=	17·5 dB
ANTENNA NOISE TEMPERATURE	=	108 KELVIN
POWER GAIN	=	35 dB
TARGET RADAR CROSS SECTION	=	1 METRE^2
DIELECTRIC CONSTANT OF SEA		
(REAL PART)	=	64·347
(IMAGINARY PART)	=	36·146
RECEIVING LINE LOSSES	=	4 dB
POLARIZATION	=	h
SEA STATE (DOUGLAS SCALE)	=	3
TEMPERATURE AT SEA LEVEL	=	30 DEGREES CELSIUS
SEA LEVEL HUMIDITY	=	80%
ATMOSPHERIC ATTENUATION	=	0·029893 dB/n.m.

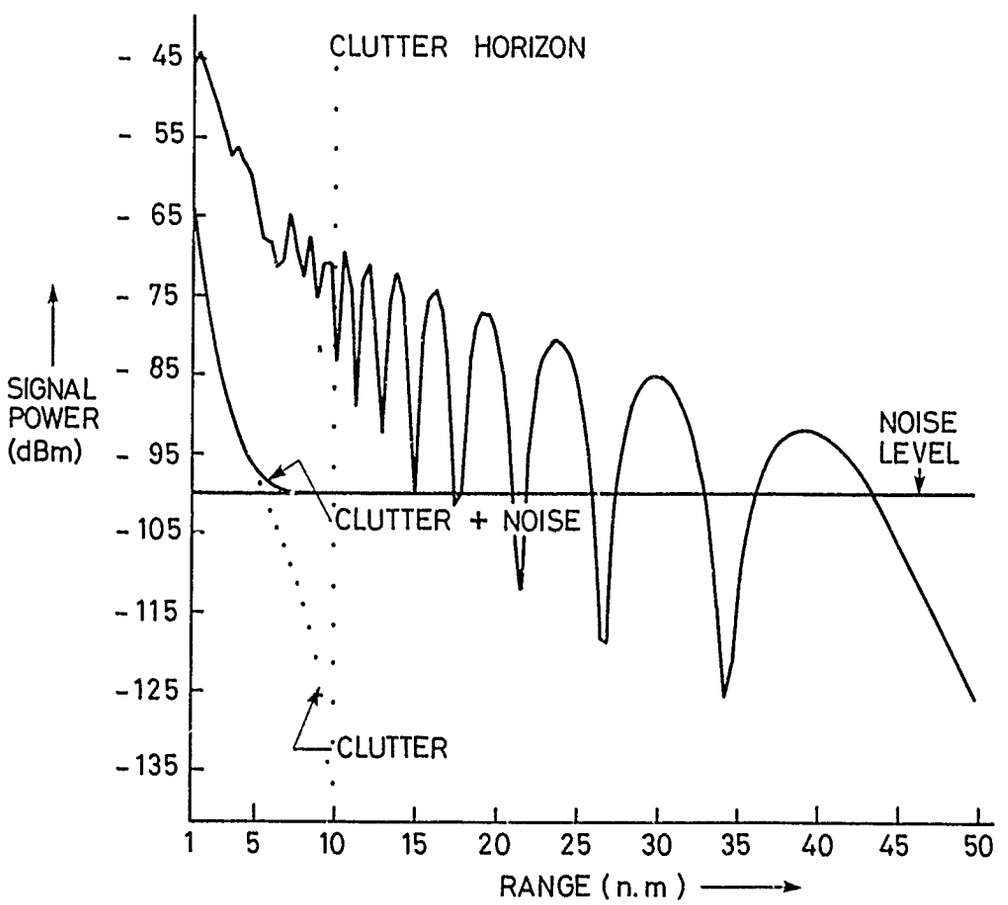

Fig. 9. 5 GHz radar return for 1m² target at 1000 ft. T=30°, humidity=80% and state 3.

FREQUENCY	=	5000 MHz
PEAK POWER	=	250 kW
RECEIVER NOISE FIGURE	=	10 dB
COMPRESSED PULSE WIDTH	=	1 MICROSEC
RADIATED PULSE WIDTH	=	1 MICROSEC
ANTENNA HEIGHT	=	50 FEET
ANTENNA TILT	=	2 DEGREES
HORIZONTAL BEAM WIDTH	=	1 DEGREE
VERTICAL BEAM WIDTH	=	10 DEGREES
VERTICAL SIDELOBE LEVEL	=	17·5 dB
ANTENNA NOISE TEMPERATURE	=	71 KELVIN
POWER GAIN	=	35 dB
TARGET RADAR CROSS SECTION	=	1 METRE ^ 2
DIELECTRIC CONSTANT OF SEA		
(REAL PART)	=	64·347
(IMAGINARY PART)	=	36·146
RECEIVING LINE LOSSES	=	4 dB
POLARIZATION	=	h
SEA STATE (DOUGLAS SCALE)	=	3
TEMPERATURE AT SEA LEVE	=	30 DEGREES CELSIUS
SEA LEVEL HUMIDITY	=	10 %
ATMOSPHERIC ATTENUATION	=	0·017670 dB/n m.

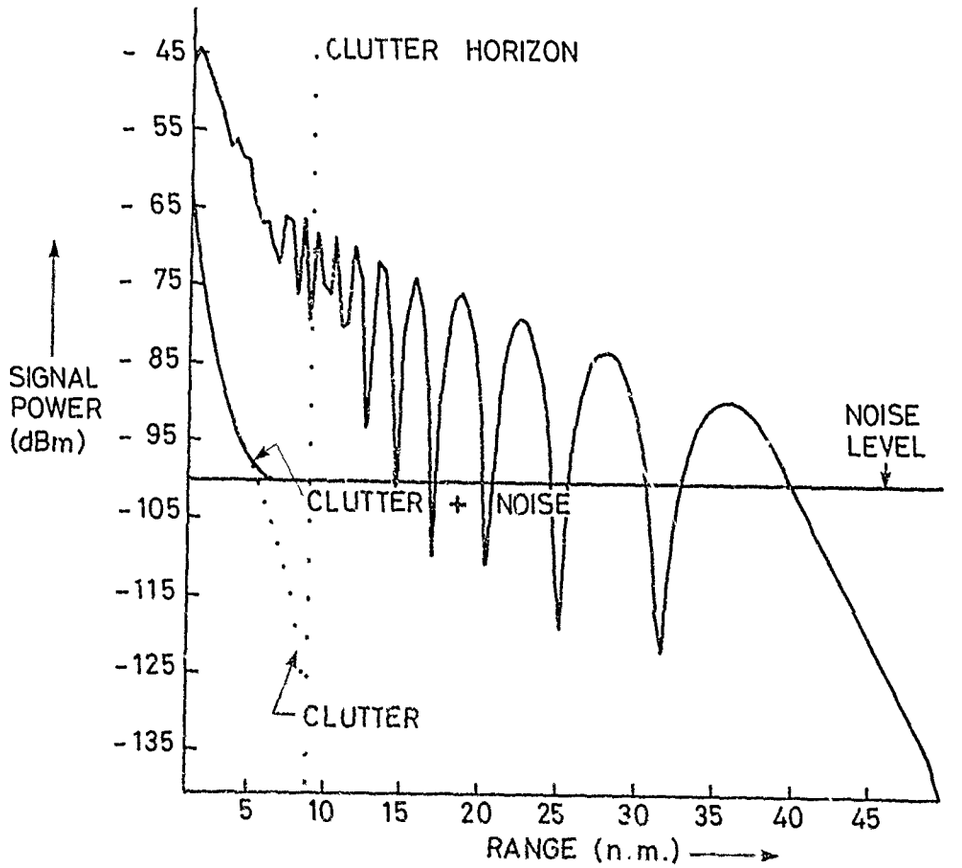

Fig. 10. 5 GHz radar return for $1 m^2$ target at 1000 ft. T = 30°, humidity = 10% and sea state 3.

Figures 11 and 12 show the effect of sea state on the radar described above. Standard conditions are assumed with sea states 0 and 5 respectively. The clutter routine used is based on a semi-empirical fit to Nathanson's data (ref 6) averaged over wind direction, as shown in the sample plot of figure 19. A small return at sea state zero is a result of the minimum wave height (0.25 ft) considered in the subroutine, which also agrees with Nathanson's data for sea state zero.

For target ranges between 5 and 30 n.miles the main effect of the increased sea state is to reduce the multipath reflectivity. This corresponds to the region of maximum slope for the roughness factor in figure 8 and results in an 8 dB reduction in the signal level for the lobe maxima. The practical result is that the detection range for a 1 square metre, 1000 ft target varies between 25 and 50 n.miles with normal variations in environmental parameters and system degradation.

At UHF frequencies the sea-state dependence of signal return is important only for higher elevation angles. Figures 13 and 14 show the variations in signal return for a sphere droped from 20,000 ft at 10 n.miles ground range, which is a typical VCD calibration profile. Above 4,000 ft the low sea state returns are 5-10 dB higher. A Gaussian model for the roughness factor (r) predicts 1-2 dB less lobing (figure 15) for high sea states than the model used here. Figure 8 suggests that at higher frequencies this would be about 3 dB.

5 PROBABILITY OF DETECTION

A second program uses the calculated signal, clutter and noise power levels to compute probability of detection for a single scan with either operator- or auto-detection. This is the same as the blip-scan ratio with unity operator efficiency if the integration time is less than the scan time of the antenna, but greater than the time required to scan one beamwidth. The main routines are listed in Annex II and described in detail in reference 2.

Target fluctuation is synthesized by using a generalized chi-squared function with distribution parameter K, which may take any value greater than zero. Non-fluctuating targets correspond to $K \gg N$ where N is the number of pulses integrated. Weinstock cases are incorported using $0.3 < K < 2.0$, and Swerling cases I-IV using $K=1, N, 2, 2N$ respectively.

FREQUENCY	= 5000 MHz
COMPRESSED PULSE WIDTH	= 1 MICROSEC
RADIATED PULSE WIDTH	= 1 MICROSEC
ANTENNA HEIGHT	= 50 FEET
ANTENNA TILT	= 2 DEGREES
HORIZONTAL BEAM WIDTH	= 1 DEGREE
VERTICAL BEAM WIDTH	= 10 DEGREES
ANTENNA NOISE TEMPERATURE	= 87 KELVIN
TARGET RADAR CROSS SECTION	= 1 METRE ^ 2
DIELECTRIC CONSTANT OF SEA	
(REAL PART)	= 66·644
(IMAGINARY PART)	= 35·883
RECEIVING LINE LOSSES	= 4 dB
POLARIZATION	= h
SEA STATE (DOUGLAS SCALE)	= 0
TEMPERATURE AT SEA LEVEL	= 15 DEGREES CELSIUS
SEA LEVEL HUMIDITY	= 60 %
ATMOSPHERIC ATTENUATION	= 0·02267 dB/n.m.

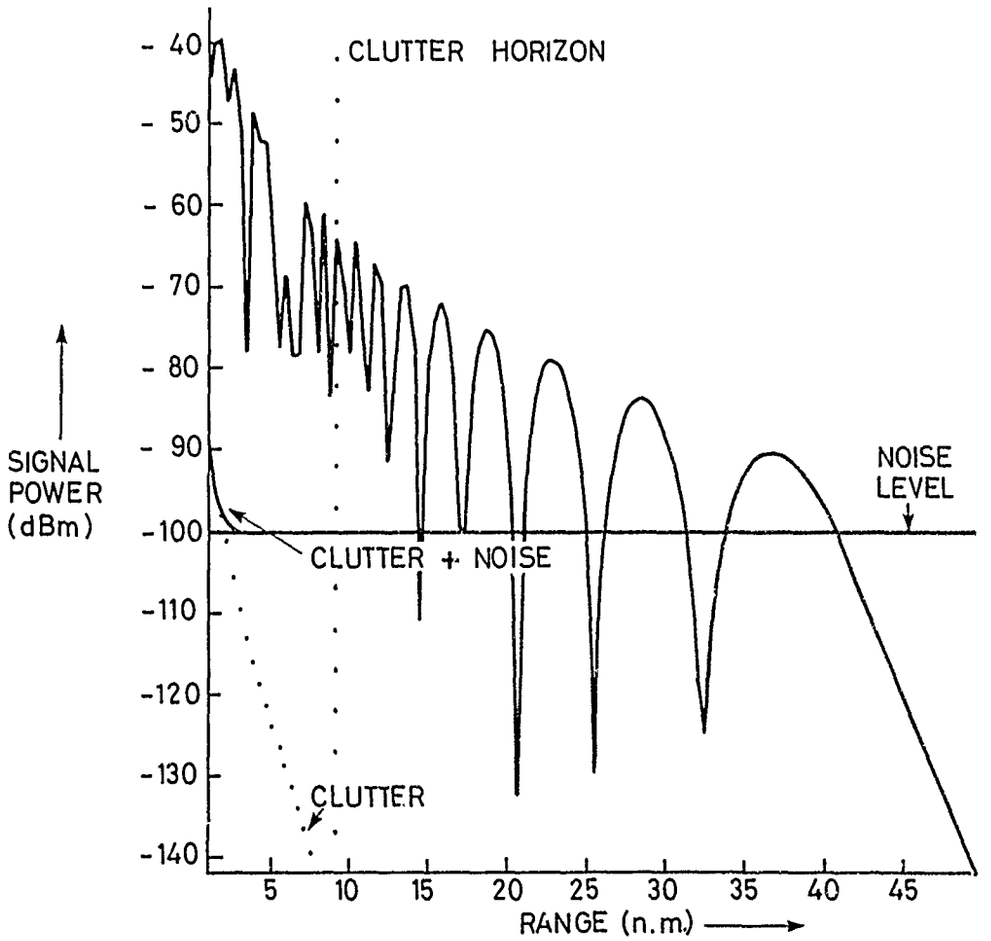

Fig. 11. 5 GHz. radar return for 1 m^2 target at 1000 ft. T = 15°, humidity = 60 % and sea state 0.

FREQUENCY	= 5000 MHz
PEAK POWER	= 250 kW
RECEIVER NOISE FIGURE	= 10 dB
COMPRESSED PULSE WIDTH	= 1 MICROSEC
RADIATED PULSE WIDTH	= 1 MICROSEC
ANTENNA HEIGHT	= 50 FEET
ANTENNA TILT	= 2 DEGREES
HORIZONTAL BEAM WIDTH	= 1 DEGREE
VERTICAL BEAM WIDTH	= 10 DEGREES
ANTENNA NOISE TEMPERATURE	= 87 KELVIN
TARGET RADAR CROSS SECTION	= 1 METRE^2
DIELECTRIC CONSTANT OF SEA	
(REAL PART)	= 66·644
(IMAGINARY PART)	= 35·883
RECEIVING LINE LOSSES	= 4 dB
POLARIZATION	= h
SEA STATE (DOUGLAS SCALE)	= 5
TEMPERATURE AT SEA LEVEL	= 15 DEGREES CELSIUS
SEA LEVEL HUMIDITY	= 60 %
ATMOSPHERIC ATTENUATION	= 0·02267 dB/n.m.

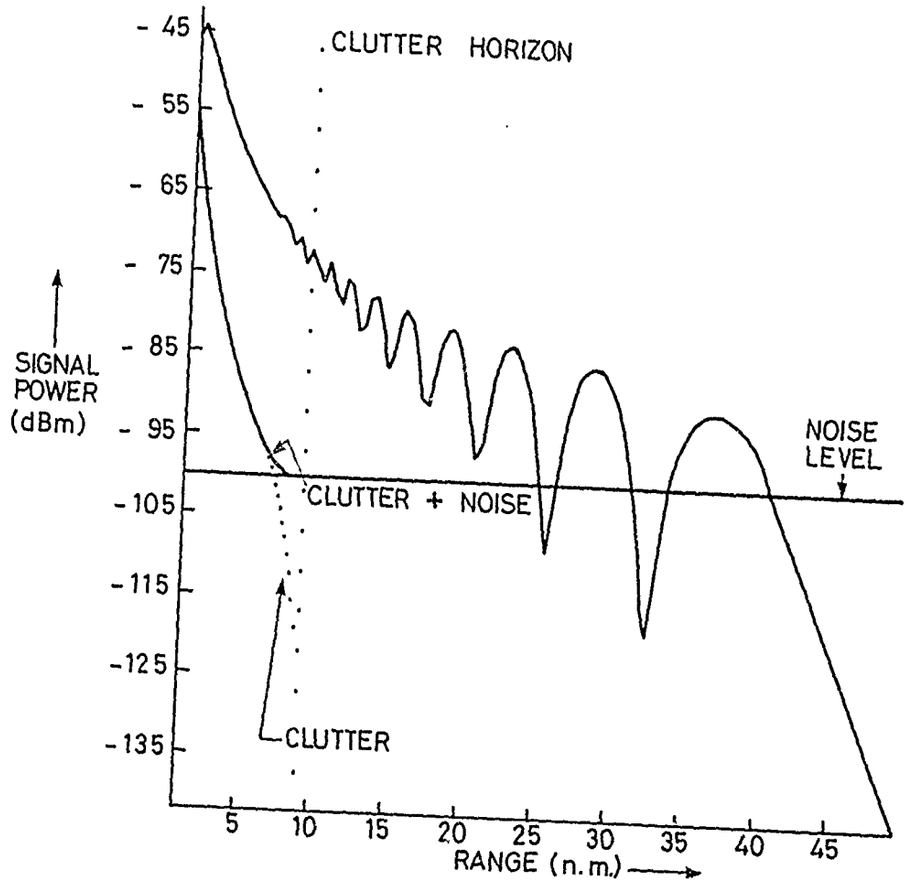

Fig. 12. 5 GHz radar return for $1m^2$ target at 1000 ft. T = 15°, humidity = 60 % and sea state 5.

FREQUENCY	=	500 MHz
PEAK POWER	=	250 kW.
RECEIVER NOISE FIGURE	=	5 dB
COMPRESSED PULSE WIDTH	=	1 MICROSECS
RADIATED PULSE WIDTH	=	1 MICROSECS
ANTENNA HEIGHT	=	100 FEET
ANTENNA TILT	=	0 DEGREES
HORIZONTAL BEAM WIDTH	=	10 DEGREES
VERTICAL BEAM WIDTH	=	20 DEGREES
VERTICAL SIDELOBE LEVEL	=	17·5 dB
ANTENNA NOISE TEMPERATURE	=	139 KELVIN
POWER GAIN	=	22 dB
TARGET RADAR CROSS SECTION	=	1 METRE ^ 2
DIELECTRIC CONSTANT OF SEA		
(REAL PART)	=	73·317
(IMAGINARY PART)	=	166·176
RECEIVING LINE LOSSES	=	5 dB
POLARIZATION	=	h
SEA STATE (DOUGLAS SCALE)	=	5
TEMPERATURE AT SEA LEVEL	=	15 DEGREES CELSIUS
SEA LEVEL HUMIDITY	=	60%
ATMOSPHERIC ATTENUATION	=	0·007073 dB/n.m

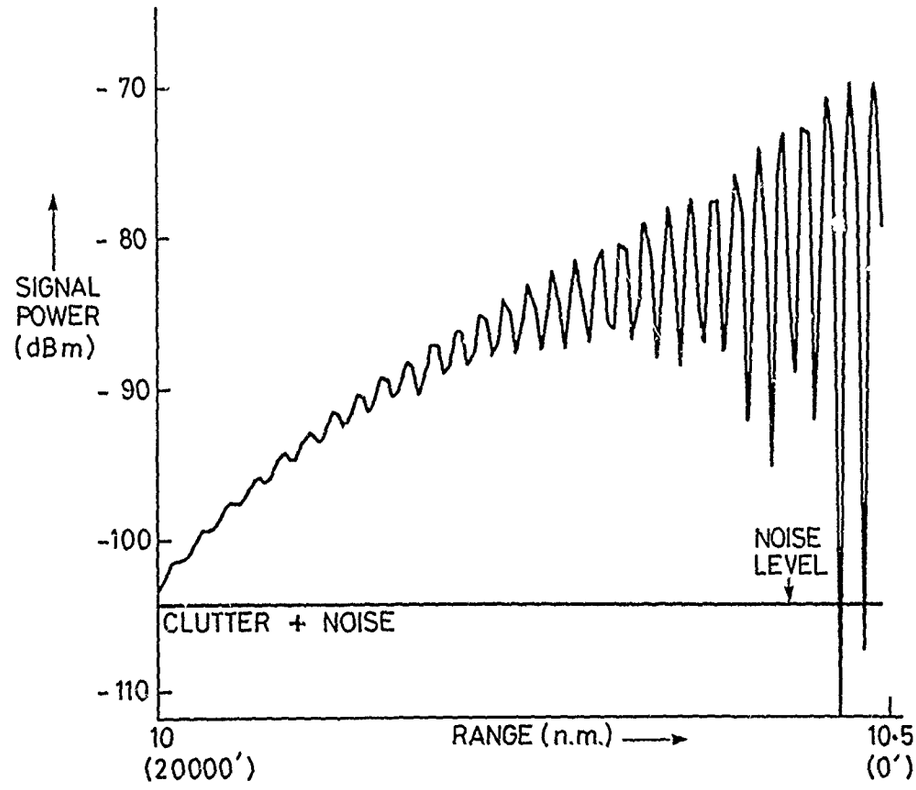

Fig. 13. UHF radar return for vertical sphere drop at 10 n. miles. Relative drift = 1 n. mile per 40 K feet, sea state 5.

FREQUENCY	=	500 MHz
PEAK POWER	=	250 kW
RECEIVER NOISE FIGURE	=	5 dB
COMPRESSED PULSE WIDTH	=	1 MICROSEC
RADIATED PULSE WIDTH	=	1 MICROSEC
ANTENNA HEIGHT	=	100 FEET
ANTENNA TILT	=	0 DEGREES
HORIZONTAL BEAM WIDTH	=	10 DEGREES
VERTICAL BEAM WIDTH	=	20 DEGREES
VERTICAL SIDELOBE LEVEL	=	17·5 dB
ANTENNA NOISE TEMPERATURE	=	139 KELVIN
POWER GAIN	=	22 dB
TARGET RADAR CROSS SECTION	=	1 METRE^2
DIELECTRIC CONSTANT OF SEA		
(REAL PART)	=	73·317
(IMAGINARY PART)	=	166·176
RECEIVING LINE LOSSES	=	5 dB
POLARIZATION	=	h
SEA STATE (DOUGLAS SCALE)	=	0
TEMPERATURE AT SEA LEVEL	=	15 DEGREES CELSIUS
SEA LEVEL HUMIDITY	=	60 %
ATMOSPHERIC ATTENUATION	=	0·007073 dB / n.m.

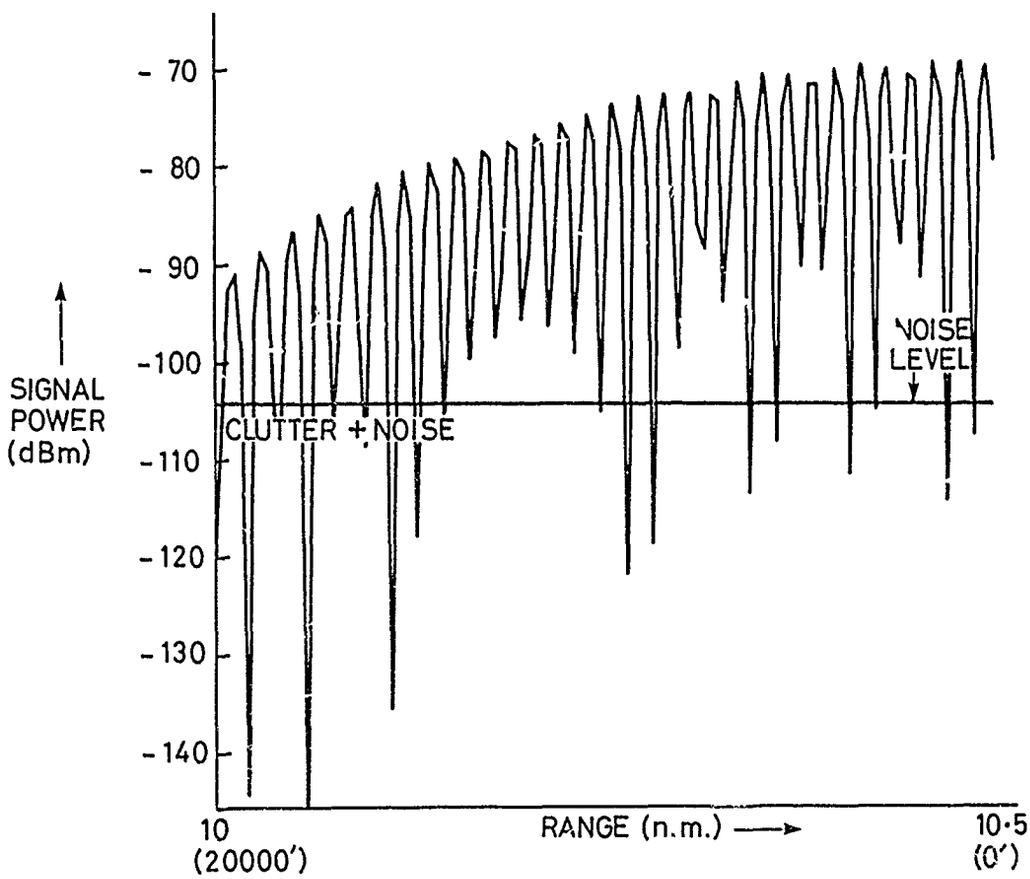

Fig. 14. UHF radar return for vertical sphere drop, sea state 0.

FREQUENCY	= 500 MHz
PEAK POWER	= 250 kW
RECEIVER NOISE FIGURE	= 5 dB
COMPRESSED PULSE WIDTH	= 1 MICROSEC
RADIATED PULSE WIDTH	= 1 MICROSEC
ANTENNA HEIGHT	= 100 FEET
ANTENNA TILT	= 0 DEGREES
HORIZONTAL BEAM WIDTH	= 10 DEGREES
VERTICAL BEAM WIDTH	= 20 DEGREES
VERTICAL SIDELOBE LEVEL	= 17·5 dB
ANTENNA NOISE TEMPERATURE	= 139 KELVIN
POWER GAIN	= 2.2 dB
TARGET RADAR CROSS SECTION	= 1 METRE^2
DIELECTRIC CONSTANT OF SEA	
(REAL PART)	= 73·317
(IMAGINARY PART)	= 166·176
RECEIVING LINE LOSSES	= 5 dB
POLARIZATION	= h
SEA STATE (DOUGLAS SCALE)	= 5
TEMPERATURE AT SEA LEVEL	= 15 DEGREES CELSIUS
SEA LEVEL HUMIDITY	= 60%
ATMOSPHERIC ATTENUATION	= 0·007073 dB/n.m.

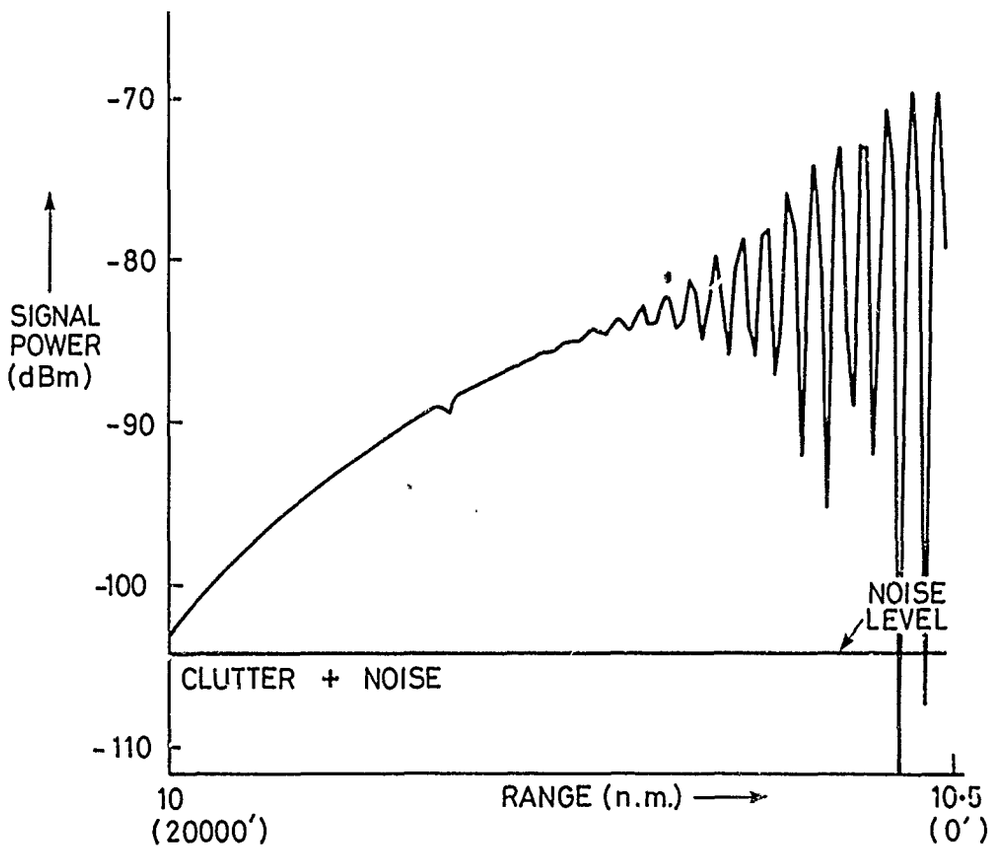

Fig. 15. U H F radar return for vertical sphere drop, sea state 5, gaussian roughness factor.

Figures 16 and 17 are plots of the output of this program for processed S/N ratios -15 to 30 dB and typical values of N=10 pulses and PFA=10^{-6}. Figure 17 shows the results for the slowly fluctuating Weinstock targets. At 90% probability of detection there is 10-20 dB difference in the required signal-to-noise ratio amongst these typical target types. That is to say, the measured VCD contour refers only to the class of target used in the VCD calibration. The difference is considerably less if R_{50} is used.

A sample of the graphical output of program II is given in figure 18 for the 5 GHz radar of figures 9-12, under standard atmospheric conditions, and incorporating the additional losses described in section 2.4. The detection probability beyond the clutter horizon (9 n.miles) is dominated by receiver noise considerations, while there is nearly 100% probability of paint at shorter ranges due to the high signal-to-clutter ratio.

Program II assumes Rayleigh statistics for surface clutter. Over the range in which this is a valid assumption ($\tau > 0.25$ μSec, $\theta_H >$ 1 degree), the clutter subroutines give $\pm$ 5 dB agreement which is of the order of the source data accuracy. This level of agreement is acceptable considering the wide range of clutter RCS encountered in routine calculations (figure 19).

ACKNOWLEDGEMENTS

Programming assistance from Lt Cdr P.Williams, RAN is gratefully acknowledged.

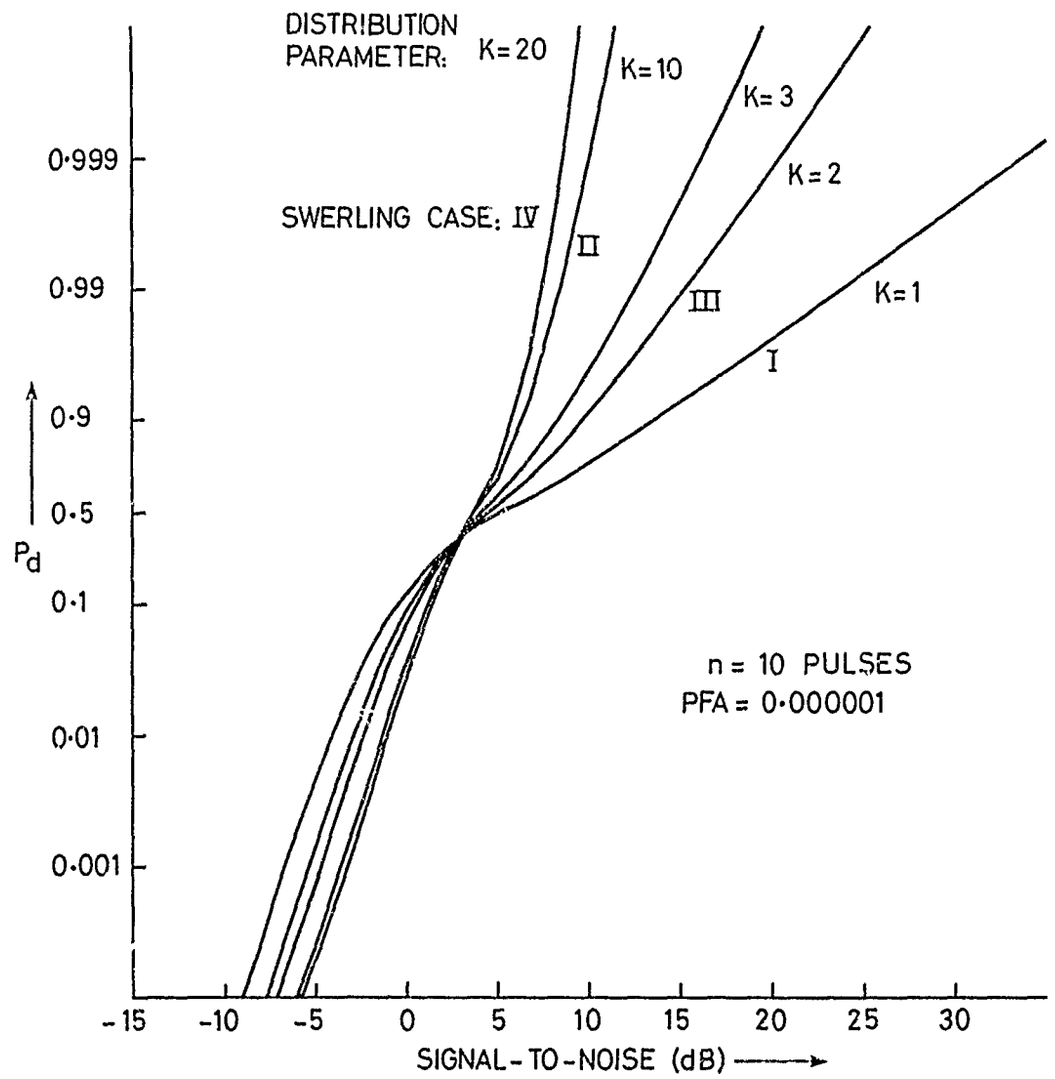

Fig. 16. Blip-scan ratio for fluctuating targets. Swerling cases I-IV and one generalized chi-square case (K=3).

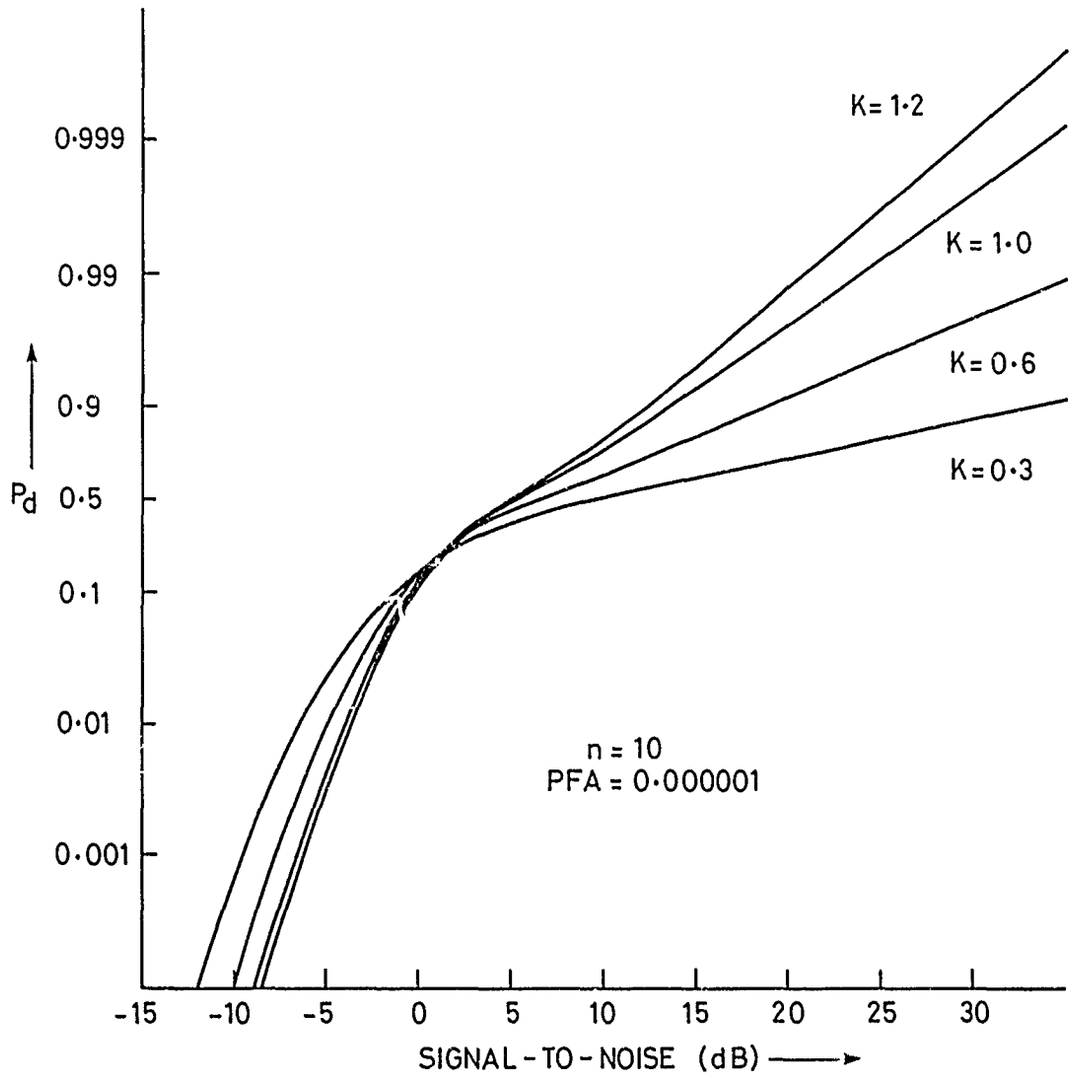

Fig. 17. Blip-scan ratio for Weinstock targets with non-integer values of K.

ANTENNA ROTATION RATE	= 10 RPM
PULSE REPETITION FREQ.	= 600 Hz.
HORIZONTAL BEAMWIDTH.	= 1 degree
FALSE ALARM PROBABILITY	= 1·0 E-6
TARGET FLUCTUATION	= SWERLING CASE 3.
BANDWIDTH MISMATCH	= 2·3 dB
DETECTOR	= OPERATOR.

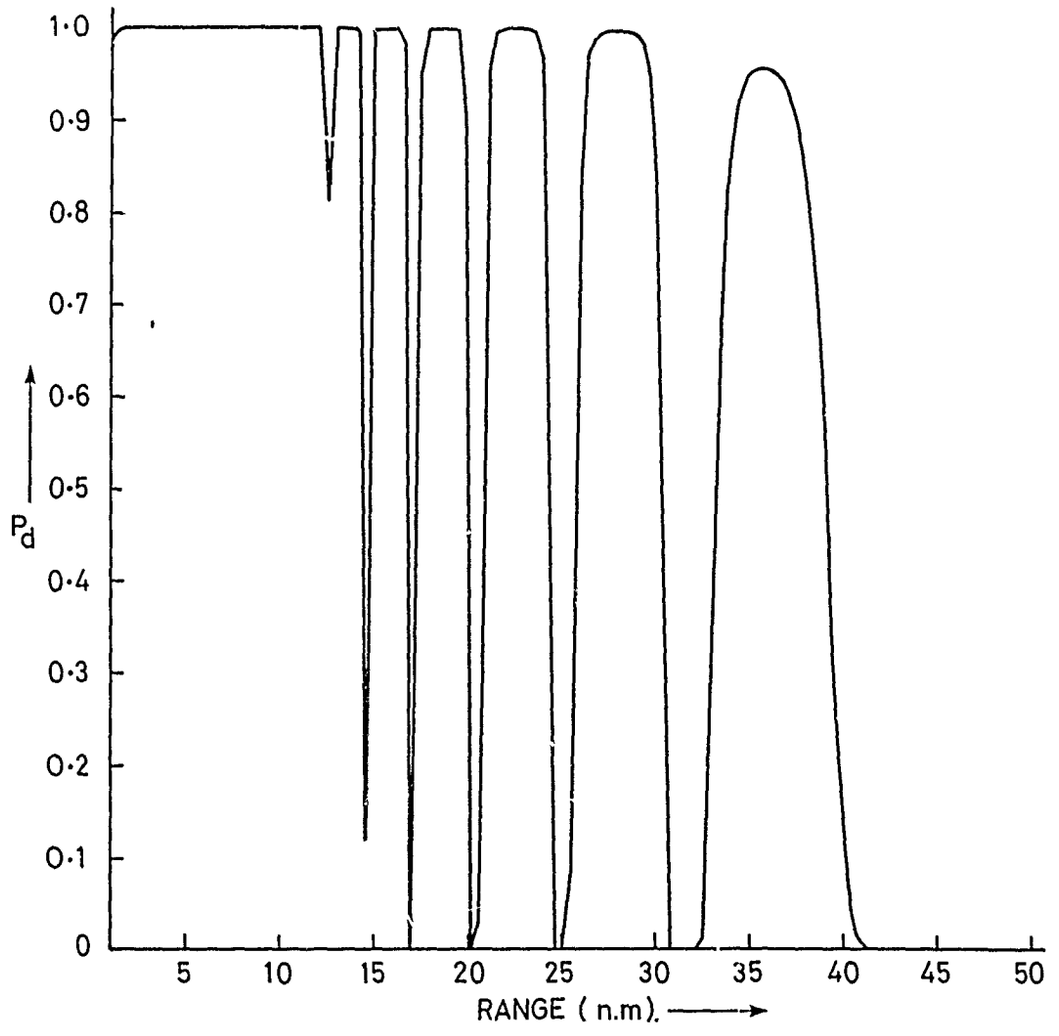

Fig. 18. Blip-scan ratio using radar parameters from figures 9-12, under standard atmospheric conditions, sea state 3.

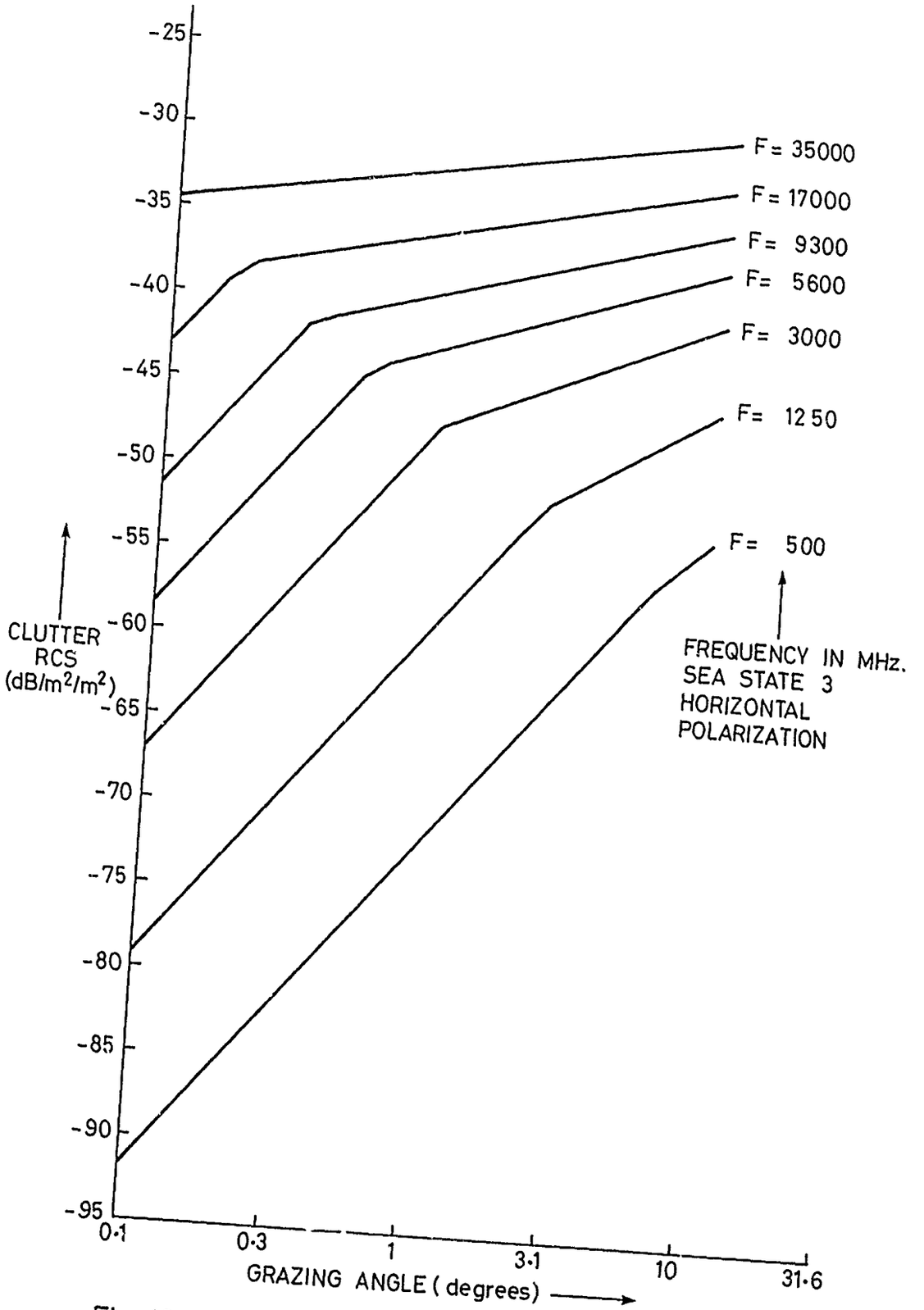

Fig. 19. Illustration of grazing-angle dependence of clutter RCS.

Wind Waves at Sea

WIND VELOCITY: (KNOTS)	4 5 6 7 8 9 10 20 30 40 50 60 70
BEAUFORT WIND AND DESCRIPTION:	1 LIGHT AIR; 2 LIGHT BREEZE; 3 GENTLE BREEZE; 4 MODERATE BREEZE; 5 FRESH BREEZE; 6 STRONG BREEZE; 7 8 9 10 11 ---- GALES --- STORM
REQUIRED FETCH (N.MILES):	50 100 200 300 400 700
REQUIRED WIND DURATION (HRS):	5 20 25 30 35
IF THE FETCH AND DURATION ARE AS GREAT AS INDICATED ABOVE THE FOLLOWING WAVE CONDITIONS WILL EXIST. WAVE HEIGHTS MAY BE UP TO 10% GREATER IF FETCH AND DURATION ARE GREATER.	
WAVE HEIGHT - $H_{1/3}$ IN FEET (CREST TO TROUGH)	1 2 4 6 8 10 15 20 25 30 40 50 60
SEA STATE AND DESCRIPTION:	1 SMOOTH; 2 SLIGHT; 3 MOD-ERATE; 4 ROUGH; 5; 6 HIGH; 7 VERY HIGH; 8 PRECIPITOUS
WAVE PERIOD (SEC):	1 2 3 4 6 8 10 12 14
WAVE LENGTH (FEET):	20 40 60 80 100 200 300 400 600 1000
WAVE VELOCITY (KNOTS):	5 10 15 20 25 30 35 40 50
PARTICLE VELOCITY: (FT/SEC)	1 2 3 4 5 6 8 10 12 14
WIND VELOCITY: (KNOTS)	4 5 6 7 8 9 10 20 30 40 50 60 70

Figure 20: Relationships between environmental parameters for waves generated by local wind. (Source: reference 6)

REFERENCES

1. Blake, L.V. (1980). Radar Range Performance Analysis, D.C.Heath and Co., Lexington.

2. Battaglia, M.R. and P.Williams (1983). RAN Research Laboratory. A Model of Radar Propagation and Detection.(U) RANRL Tech Note (Ext) 2/83. UNCLASSIFIED.

3. Kerr, D.E.(Ed.) (1951). Propagation of Short Radio Waves. M.I.T. Radiation Lab Series, Vol 13, McGraw-Hill, New York.

4. Barton, D.K. (1964). Radar System Analysis, Prentice-Hall, New Jersey.

5. Skolnik, M.I.(Ed.) (1970). The Radar Handbook, McGraw-Hill, New York.

6. Nathanson, F.E. (1969). Radar Design Principles, McGraw-Hill, New York.

ANNEX I: Antenna Pattern Functions

The required inputs for the antenna pattern function routines are i) 3dB beamwidths, ii) level of first sidelobe and iii) pencil or cosecant-squared pattern. Pencil patterns are calculated according to the normalized functions

$$f(\theta) = \frac{\sin \pi(u^2-B^2)^{0.5}}{f_o \pi(u^2-B^2)^{0.5}} \qquad \text{I-1}$$

with

$$f_o = \frac{\sinh \pi B}{\pi B}$$

or equivalently

$$f(\theta) = \frac{\sinh \pi(B^2-u^2)^{0.5}}{f_o \pi(B^2-u^2)^{0.5}} \qquad \text{I-2}$$

where $u=d.\sin\theta/\lambda$ and B is related to the sidelobe voltage ratio η

$$\eta = 4.603\frac{\sinh \pi B}{\pi B} \qquad \text{I-3}$$

B=0 corresponds to a sin x/x pattern with 13.26 dB sidelobe. The BASIC version of the program uses a cubic fit of tabulated solutions for the above relation and for the aperture efficiency. The numerical accuracy is comparable with that of the recursive algorithm described in reference 2. Aperture blockage is not calculated explicitly but can be approximated using observed sidelobe levels and a cosec weighting factor as plotted in figure I-1. This is equivalent to assuming that the envelope decays as 1/u after the obstacle contribution is added. Since simple parametric forms of $f(\theta)$ are generally adequate only for the first few sidelobes, this treatment should be reasonable for a first-order correction.

The program is easily modified to use a lambda function subroutine for $f(\theta)$. This form is appropriate for an aperture with distribution $[1-(r/r_o)^2]^{\alpha-1}$ so that f(u) is a lambda function of the first kind

$$f(u) = 2^{\alpha}\Gamma(1+\alpha)\frac{J_{\alpha}(u)}{u^{\alpha}} \qquad \text{I-4}$$

where $J_{\alpha}(u)$ is the Bessel function of order α. The subroutine uses a truncation of the infinite series for $J_{\alpha}(u)$. Figure I-2 shows the output of this subroutine, with the series truncated at u^{100} for α= 0.5 (sin x/x), α= 1.0 (uniformly illuminated circular aperture) and α= 2.0. Circular apertures typically have α>1.0 (V>17.6 dB). Apart from computational simplicity, the reason that the modified sin u/u pattern is the default form for $f(\theta)$ is illustrated in figure I-3 where the infinite series has been truncated at u^{2n} for n = 10,15,20 and 50. There is negligible difference in the position of the first sidelobe for the two expressions. The main difference is that the sidelobe return for the Bessel function form diverges rapidly beyond the first sidelobe unless a large number of terms is included. This is not convenient for routine calculations.

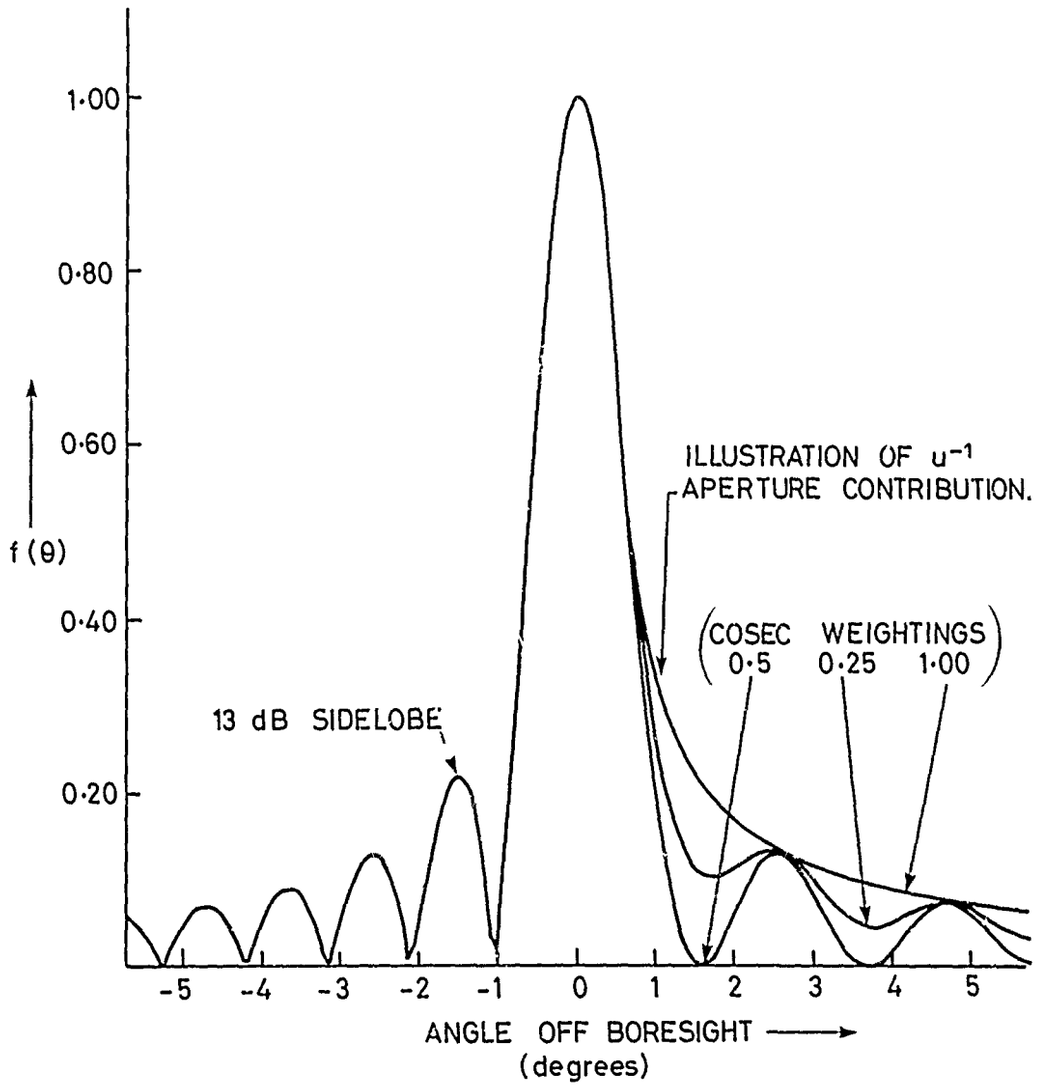

Fig. I-1. Modified sin u/u antenna pattern function for $\theta = 1^{\circ}$, $B = 0$.

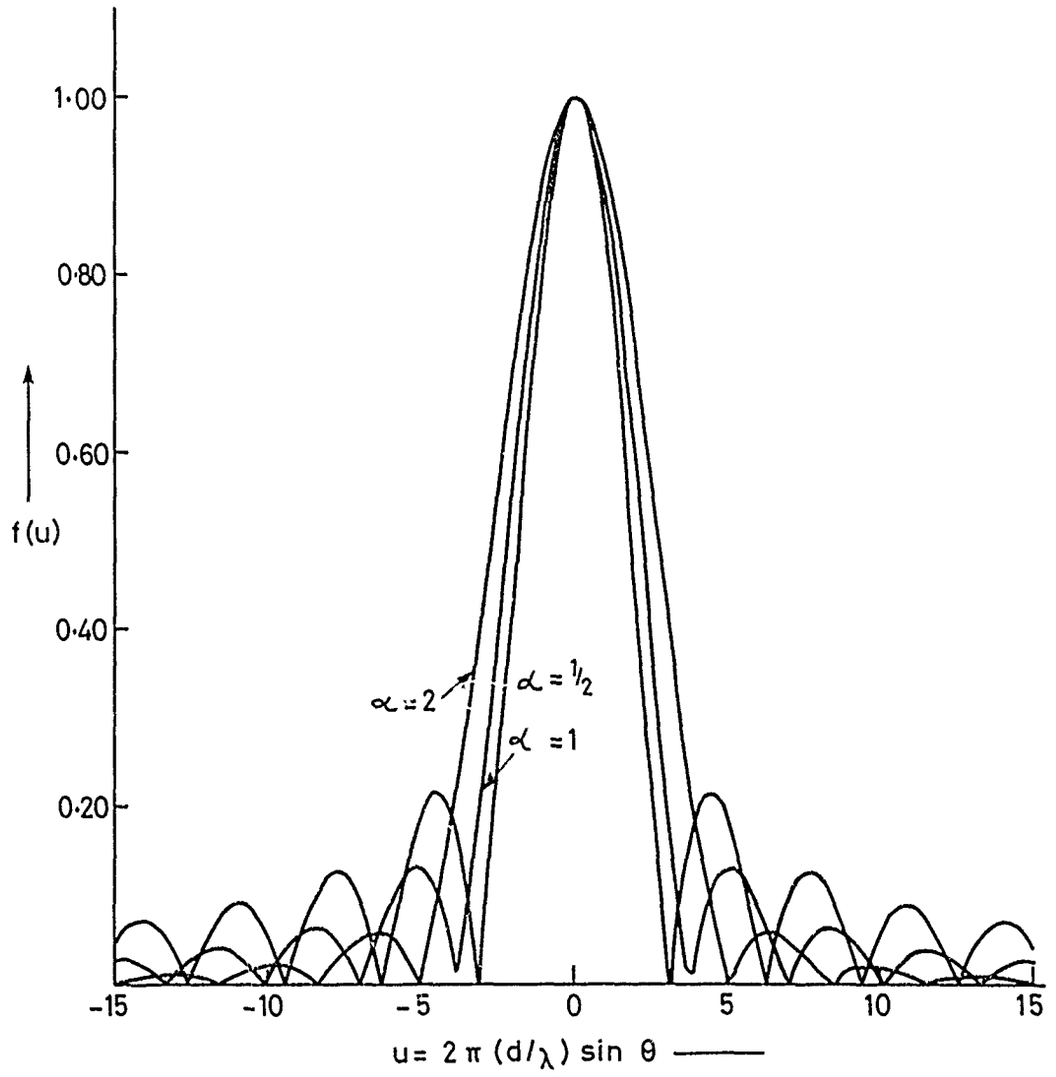

Fig. I-2. Normalized Bessel functions ($J_\alpha(u)/u^\alpha$) for $\alpha = 0{\cdot}5, 1, 2$ calculated from series truncated at u^{100}.

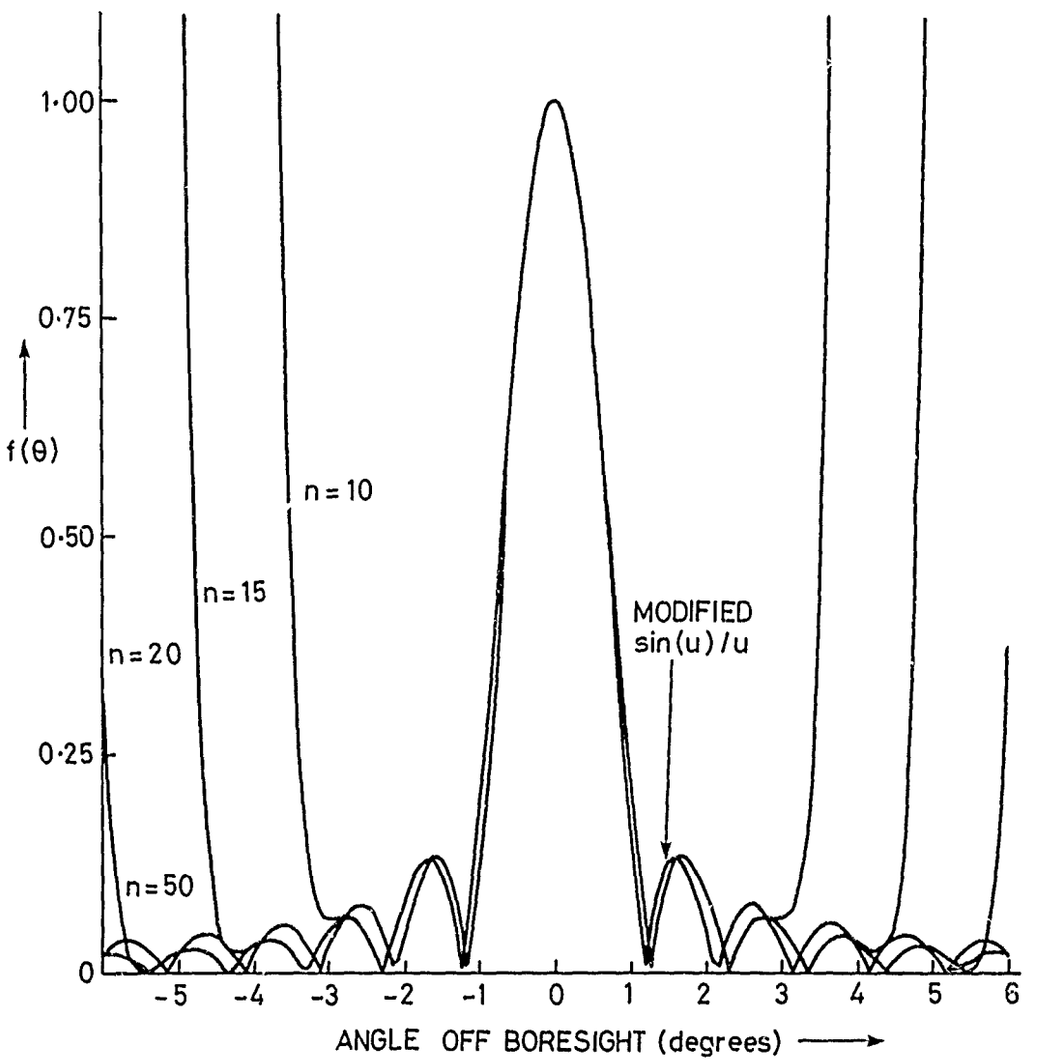

Fig. I-3. Normalized Bessel function ($J_1(u)/u$) with series truncated at u^{2n} with n =10, 15, 20 and 50. Modified sin u/u with 17·6 dB sidelobe shown for comparison. BW = 1°.

Annex II:

Probability of Detection Subroutines
for Generalized Chi-squared Target

```
1180 REM  I/P to 1st subroutine (1320) is PFA (P0),number of pulses int'd (N)
1190 REM 1st subroutine is used to calculate threshold for fixed threshold det'r
1195 REM ##########################################################################
1210 Y1=EXP(-Y0)
1220 Y2=Y1
1230 N0=1
1240 IF N<=1 THEN 1290
1250 Y1=Y1*Y0/N0
1260 Y2=Y2+Y1
1270 N0=N0+1
1280 IF N0<N THEN 1250
1290 RETURN
1300 REM
1310 REM
1315 REM ##########################################################################
1320 REM Start of first routine which calculates threshold (Y0) from PFA (P0)
1330 Y0=-1*LOG(P0)
1340 IF N<=1 THEN 1410
1350 REM First estimate for Y0
1360 Y0=(SQR(-LOG(P0))+SQR(N)-1)*SQR(-LOG(P0))+N-SQR(N)
1370 GOSUB 1210
1380 D0=LOG(Y2/P0)*Y2/Y1
1390 Y0=Y0+D0
1400 IF ABS(D0/Y0)=>3.0E-7 THEN 1370
1410 REM Y0 is threshold for fixed threshold detector
1420 RETURN
1425 REM ##########################################################################
1430 REM Start of routine to calculate Pd from signal-to-noise (X)
1440 GOSUB 1210
1450 X=10^(X/10)
1460 S1=Y2
1470 X1=(K/(K+N*X))^K
1480 X2=X1
1490 X3=X*N/(K+N*X)
1500 D1=K-1
1510 M=1
1520 R1=0
1530 L1=R1
1540 Y1=Y1/N0*Y0
1550 Y2=Y2+Y1
1560 S1=S1+Y1*(1-X2)
1570 E1=(1-X2)*(1-Y2)
1580 R1=S1+E1
1590 X1=(D1+M)/M*X1*X3
1600 X2=X2+X1
1610 M=M+1
1620 N0=N0+1
1630 IF ABS(1-L1/R1)=>3.0E-7 THEN 1530
1640 IF E1=>0.1 THEN 1530
1650 REM r1 is the blip-scan ratio
1660 RETURN
1700 REM ##########################################################################
```

ANNEX III: Solutions to Multipath Geometry

The pattern propagation factor of equation 8 is evaluated at all points in the interference region according to the expression

$$F = f(\theta_1)\,|[1 + x^2 + 2x\cos(\phi + 2\pi\delta/\lambda)]^{0.5}| \qquad \text{III-1}$$

where ϕ is the phase difference on reflection, λ is the wavelength and δ is the path difference for the direct and indirect rays:

$$\delta = \frac{4R_1R_2\sin^2\gamma}{R_1 + R_2 + R} \qquad \text{III-2}$$

where R, R_1 and R_2 are as shown in figure 1 of the main body of this note. To determine these slant ranges, the corresponding ground range is first evaluated

$$G_1 = G/2 - p\sin(\xi/3) \qquad \text{III-3}$$

with

$$p = \frac{2}{\sqrt{3}}\sqrt{a_e(h_1+h_2) + (G/2)^2} \qquad \text{III-4}$$

$$\xi = \sin^{-1}\frac{2a_eG(h_2-h_1)}{p^3} \qquad \text{III-5}$$

The slant range is then

$$R = \sqrt{(h_2-h_1)^2+4(a_e+h_1)(a_e+h_2)\sin^2[(G_1+G_2)/2a_e]} \qquad \text{III-6}$$

R_1 (R_2) is obtained by substituting $h_2=0$ ($h_1=0$) and $G_2=0$ ($G_1=0$). The solutions for θ_1, θ_2 and γ are:

$$\theta_1 = \sin^{-1}\frac{2a_e(h_2-h_1)+h_2^2-h_1^2-R^2}{2(a_e+h_1)R} \qquad \text{III-7}$$

$$\theta_2 = \sin^{-1}\frac{2a_eh_1+h_1^2+R_1^2}{2(a_e+h_1)R_1} \qquad \text{III-8}$$

$$\gamma = \sin^{-1}\frac{2a_eh_1+h_1^2-R_1^2}{2a_eR_1} \qquad \text{III-9}$$

DISTRIBUTION	COPY NO.
Chief Defence Scientist	1
Deputy Chief Defence Scientist	2
CPAS	3
SSTP	4
JIO (DSTI)	5
RANRL Library master copy	6
Counsellor Defence Science, Washington	7
Defence Science Rep. London	8
Librarian Technical Reports Centre, Defence Central Library, Campbell Park	9
OIC Document Exchange Centre DISB	10 - 27
Director of Operational Analysis - Navy	28
Director of Surface and Air Weapons - Navy	29
Director of Electronic Warfare - Navy	30
Naval Scientific Adviser	31
Officer-in-Charge RAN Trials and Assessing Unit	32
Director RAN Tactical School, HMAS WATSON	33
Senior Librarian, Defence Research Centre Salisbury	34
Senior Librarian, Aeronautical Research Laboratories	35
Librarian H Block, Victoria Barracks, Melbourne	36
Dr M. R. Battaglia	37
Lt Cdr P. Williams, RAN	38
RANRL Library	39 - 43

DOCUMENT CONTROL DATA SHEET

1. a. A.R. No.	1.b. Establishment No.	2. Document Date	3. Task No
002-707	RANRL Tech Note (External) 1/83	March 1983	A8/81

4. Title	5. Security	6.No Pages
A Computer Program for the Prediction of Search Radar Performance.	a. document UNCLAS b. title UNCLAS c. abstract UNCLAS	40 7.No Refs 6

8. Author(s)	9.Downgrading Instructions
BATTAGLIA M.R.	N/A

10. Corporate Author and Address	11.Authority (as appropriate)
RAN Research Laboratory P.O. Box 706, Darlinghurst. N.S.W. 2010	a.Sponsor b. Security c.Downgrading d.Approval a.Operations Research Div. b.HORD c.N/A (unclass) d.W.F. Hunter,Director RANRL W.F. Hunter.

12. Secondary Distribution (of this document)

Approved for Public Release

13. a. This document may be ANNOUNCED in catalogues and awareness services available to :

No limitations

13. b. Citation for other purposes (ie casual announcement) may be as for 13a.

14. Descriptors	15. COSATI Group
Radar, model, multipath,computer program attenuation, detection	17090

16. Abstract

A computer program is described which calculates signal and clutter return and probability of detection for scanning search radars. Sample outputs are plotted showing the effects of humidity, sea state and target scintillation.